

# Exploring the advantages of multiband fMRI with simultaneous EEG to investigate coupling between gamma frequency neural activity and the BOLD response in humans

Uji, Makoto; Wilson, Ross; Francis, Susan; Mullinger, Karen; Mayhew, Stephen

DOI:  
[10.1002/hbm.23943](https://doi.org/10.1002/hbm.23943)

License:  
Other (please specify with Rights Statement)

Document Version  
Peer reviewed version

Citation for published version (Harvard):  
Uji, M, Wilson, R, Francis, S, Mullinger, K & Mayhew, S 2018, 'Exploring the advantages of multiband fMRI with simultaneous EEG to investigate coupling between gamma frequency neural activity and the BOLD response in humans', *Human Brain Mapping*, vol. 39, no. 4, pp. 1673-1687. <https://doi.org/10.1002/hbm.23943>

[Link to publication on Research at Birmingham portal](#)

## Publisher Rights Statement:

This is the peer reviewed version of the following article: Uji M, Wilson R, Francis ST, Mullinger KJ, Mayhew SD. Exploring the advantages of multiband fMRI with simultaneous EEG to investigate coupling between gamma frequency neural activity and the BOLD response in humans. *Hum Brain Mapp.* 2018;39:1673–1687, which has been published in final form at: <https://doi.org/10.1002/hbm.23943>. This article may be used for non-commercial purposes in accordance with Wiley Terms and Conditions for Self-Archiving.

## General rights

Unless a licence is specified above, all rights (including copyright and moral rights) in this document are retained by the authors and/or the copyright holders. The express permission of the copyright holder must be obtained for any use of this material other than for purposes permitted by law.

- Users may freely distribute the URL that is used to identify this publication.
- Users may download and/or print one copy of the publication from the University of Birmingham research portal for the purpose of private study or non-commercial research.
- User may use extracts from the document in line with the concept of 'fair dealing' under the Copyright, Designs and Patents Act 1988 (?)
- Users may not further distribute the material nor use it for the purposes of commercial gain.

Where a licence is displayed above, please note the terms and conditions of the licence govern your use of this document.

When citing, please reference the published version.

## Take down policy

While the University of Birmingham exercises care and attention in making items available there are rare occasions when an item has been uploaded in error or has been deemed to be commercially or otherwise sensitive.

If you believe that this is the case for this document, please contact [UBIRA@lists.bham.ac.uk](mailto:UBIRA@lists.bham.ac.uk) providing details and we will remove access to the work immediately and investigate.



**Exploring the advantages of multiband fMRI with simultaneous EEG to investigate coupling between gamma frequency neural activity and the BOLD response in humans.**

Journal:	<i>Human Brain Mapping</i>
Manuscript ID	HBM-17-1128.R1
Wiley - Manuscript type:	Research Article
Date Submitted by the Author:	n/a
Complete List of Authors:	Uji, Makoto; School of Psychology and BUIC, University of Birmingham Wilson, Ross; School of Psychology and BUIC, University of Birmingham Francis, Susan; SPMIC, School of Physics and Astronomy, University of Nottingham Mullinger, Karen; SPMIC, School of Physics and Astronomy, University of Nottingham; School of Psychology and BUIC, University of Birmingham Mayhew, Stephen; School of Psychology and BUIC, University of Birmingham
Keywords:	EEG-fMRI, Multiband fMRI, Gamma-BOLD coupling, Gradient artefacts, Safety, Heating, Motor gamma oscillations, Multislice fMRI

SCHOLARONE™  
Manuscripts

1  
2  
3 Exploring the advantages of multiband fMRI with simultaneous EEG to investigate coupling  
4  
5 between gamma frequency neural activity and the BOLD response in humans.  
6  
7

8  
9 Makoto Uji<sup>a</sup>, Ross Wilson<sup>a</sup>, Susan T. Francis<sup>b</sup>, Karen J. Mullinger<sup>a,b,\*†</sup>, Stephen D.  
10  
11 Mayhew<sup>a\*</sup>  
12

13 <sup>a</sup> Centre for Human Brain Health (CHBH), School of Psychology, University of Birmingham,  
14  
15 Birmingham, UK  
16

17 <sup>b</sup> Sir Peter Mansfield Imaging Centre (SPMIC), School of Physics and Astronomy, University  
18  
19 of Nottingham, Nottingham, UK  
20  
21

22 \* these authors were equally responsible for leading this study  
23

24 † corresponding author  
25  
26  
27  
28  
29  
30  
31  
32  
33  
34  
35  
36  
37  
38  
39  
40  
41  
42  
43  
44  
45  
46  
47  
48  
49  
50  
51  
52  
53  
54  
55  
56  
57  
58  
59  
60

## Abstract

We established an optimal combination of EEG recording during sparse multiband (MB) fMRI that preserves high resolution, whole brain fMRI coverage whilst enabling broad-band EEG recordings which are uncorrupted by MRI gradient artefacts (GAs). We firstly determined the safety of simultaneous EEG recording during MB fMRI. Application of MB factor=4 produced  $<1^{\circ}\text{C}$  peak heating of electrode/hardware during 20-minutes of GE-EPI data acquisition. However, higher SAR sequences require specific safety testing, with greater heating observed using PCASL with MB factor=4. Heating was greatest in the electrocardiogram channel, likely due to it possessing longest lead length. We investigated the effect of MB factor on the temporal signal to noise ratio for a range of GE-EPI sequences (varying MB factor and temporal interval between slice acquisitions). We found that, for our experimental purpose, the optimal acquisition was achieved with MB factor=3, 3mm isotropic voxels and 33 slices providing whole head coverage. This sequence afforded a 2.25s duration quiet period (without GAs) in every 3s TR. Using this sequence we demonstrated the ability to record gamma frequency (55-80Hz) EEG oscillations, in response to right index finger abduction, that are usually obscured by GAs during continuous fMRI data acquisition. In this novel application of EEG-MB fMRI to a motor task we observed a positive correlation between gamma and BOLD responses in bilateral motor regions. These findings support and extend previous work regarding coupling between neural and haemodynamic measures of brain activity in humans and showcase the utility of EEG-MB fMRI for future investigations.

## Keywords

EEG-fMRI  
Multiband or multislice fMRI  
Gamma-BOLD coupling  
Gradient artefacts  
Safety  
Heating  
Motor gamma oscillations

## Introduction

Electroencephalography (EEG) and functional magnetic resonance imaging (fMRI) are two neuroimaging techniques that are often used to investigate human brain function. Simultaneous EEG-fMRI recordings provide a wide range of complimentary information and can be advantageous for improving our understanding of brain function, for example: through investigating the spatiotemporal dynamics of neural activity (for a review, see Huster et al., 2012), or studying the underlying neurophysiological origins of the measured responses by comparing neural and haemodynamic signals e.g. (Mullinger et al., 2013). The primary advantage of simultaneous EEG-fMRI acquisition over separate recordings is that it enables investigation of unpredictable or spontaneous brain activity, as well as studying the trial-by-trial covariation in brain processing as measured by the two techniques (Bagshaw et al., 2004; Becker et al., 2011; Debener et al., 2006; Eichele et al., 2008; Goldman et al., 2002; Horovitz et al., 2008; Mayhew et al., 2013; Mobascher et al., 2009; Mullinger et al., 2014; Olbrich et al., 2009; Scheibe et al., 2010). Thus simultaneous recordings enable spatial localisation of temporally dynamic response features. EEG-fMRI analysis has provided many novel insights into brain function. For example, such analyses have demonstrated specific BOLD correlates of: distinct neurophysiological components including the auditory oddball (Bénar et al., 2007; Eichele et al., 2005) and the error-related negativity (Debener et al., 2005); as well as specific neural activity in specific frequency bands (Goldman et al., 2002; Laufs et al., 2003). These studies have shown that simultaneous EEG-fMRI can provide greater specificity regarding the spatial arrangement (Goldman et al., 2009; Novitskiy et al., 2011) or the temporal sequence (Eichele et al., 2005; Mayhew et al., 2012) of responsive brain areas, compared to that revealed by a standard analysis of data from a single neuroimaging modality.

Recently, neuronal activity in the gamma frequency band, which is typically defined as between approximately 30-100Hz, has attracted much interest because gamma

1  
2  
3 synchronization has been linked with a range of cognitive and sensory functions (Buschman  
4 and Miller, 2007; Buzsaki and Draguhn, 2004; Colgin et al., 2009; Fries, 2009; Singer and  
5 Gray, 1995). Gamma-band synchronization has been observed in humans using non-invasive  
6 imaging methods during visual (Hoogenboom et al., 2006; Muthukumaraswamy and Singh,  
7 2013), somatosensory (Bauer et al., 2006) and auditory (Pantev et al., 1991; Schadow et al.,  
8 2009) stimulation. It is also known to be involved in higher cognitive functions such as  
9 memory processes (Fell et al., 2001; Howard et al., 2003) and motor control (Brown et al.,  
10 1998; Cheyne et al., 2008; Crone et al., 1998; Darvas et al., 2010; Gaetz et al., 2010;  
11 Muthukumaraswamy, 2010; Schoffelen et al., 2005). Therefore, due to the functional  
12 importance of gamma frequency activity, characterising the underlying mechanisms of these  
13 responses is of great interest.

14  
15  
16  
17  
18  
19  
20  
21  
22  
23  
24  
25  
26  
27 The majority of previous work investigating the link between BOLD signals and gamma  
28 activity has been conducted using invasive electrode recordings of local-field potentials in  
29 humans (Mukamel et al., 2005; Murta et al., 2016; Nir et al., 2007), primates (Logothetis et  
30 al., 2001; Magri et al., 2012; Niessing et al., 2005; Scholvinck et al., 2010; Viswanathan and  
31 Freeman, 2007) and rodents (Boorman et al., 2015; Sumiyoshi et al., 2012). These studies  
32 showed the BOLD response is more strongly coupled to gamma frequency activity, compared  
33 with the activity in the lower (<30Hz) frequency bands.

34  
35  
36  
37  
38  
39  
40  
41  
42  
43 Whilst providing novel insights into neurovascular coupling, findings from invasive animal  
44 recordings cannot be easily extrapolated to scalp electrophysiological recordings due to  
45 differences in the recording references used and in the spatial scale of the neuronal  
46 populations involved in generating the signals (Hall et al., 2005). In addition, although the  
47 coupling between BOLD and gamma-LFP activity is widely cited as principle evidence for  
48 the neural underpinnings of haemodynamic based functional neuroimaging, the majority of  
49 these seminal studies have been conducted in visual cortex (Logothetis et al., 2001;  
50  
51  
52  
53  
54  
55  
56  
57  
58  
59  
60

1  
2  
3 Viswanathan and Freeman, 2007), with some exceptions in auditory cortex (Mukamel et al.,  
4 2005). A wider understanding in other brain regions, for example sensorimotor cortex, is  
5 important to fully establish the fundamental nature of the gamma-BOLD relationship. Such  
6 investigations are particularly important given the recent doubt cast on the functional  
7 importance of narrow-band gamma responses in visual cortex (Hermes et al., 2014), and the  
8 BOLD correlates of broader high-frequency activity (Winawer et al., 2013). Therefore non-  
9 invasive simultaneous EEG-fMRI recordings in humans offer many potential advantages for  
10 relating gamma and BOLD signals. Possibilities include extending previous studies  
11 suggestions of a strong gamma-BOLD relationship by investigating this coupling in motor  
12 paradigms, which have been widely shown to induce robust increases in gamma power  
13 (Cheyne et al., 2008; Crone et al., 1998; Gaetz et al., 2010; Muthukumaraswamy, 2010), and  
14 gaining a fuller understanding of the fundamental relationship of these signals to each other  
15 and also to human behaviour (Hoogenboom et al., 2010; Womelsdorf et al., 2006).

16  
17  
18  
19  
20  
21  
22  
23  
24  
25  
26  
27  
28  
29  
30  
31 However, few simultaneous EEG-fMRI studies have investigated gamma activity due to  
32 technical limitations as detailed below, and consequently the relationship between  
33 haemodynamic responses and the gamma band activity in humans remains incompletely  
34 understood (Logothetis, 2008). The recording of EEG data in the MRI environment is  
35 technically challenging primarily due to the effect of the MRI on the EEG data quality.  
36  
37  
38  
39  
40  
41  
42  
43  
44  
45  
46  
47  
48  
49  
50  
51  
52  
53  
54  
55  
56  
57  
58  
59  
60  
Namely, EEG data are corrupted by the gradient artefact (GA) produced by the time-varying  
magnetic field gradients needed for imaging, the pulse artefact produced by cardiac pulse  
driven motion in the strong magnetic field of the MR scanner, and motion artefacts due to  
head movement in the MR environment (Mullinger and Bowtell, 2011). The frequency  
characteristics of these artefacts mean that the GA is the primary problem for studying  
gamma band activity, with residual GAs easily obscuring the small amplitude neuronal signal  
of interest even after correction (Mullinger et al., 2011, 2008b).

1  
2  
3 Despite the technical challenges, a few studies have attempted to study the gamma band  
4 using concurrent EEG and fMRI measures (Castelhano et al., 2014; Green et al., 2017; Leicht  
5 et al., 2016; Mantini et al., 2007; Michels et al., 2010; Mulert et al., 2010; Rosa et al., 2010;  
6 Scheeringa et al., 2011). Of these a number limited the frequency range of the measured  
7 gamma band to a range of 30-50Hz (or narrower) to avoid the high frequencies where the  
8 GAs dominate (e.g. Mantini et al., 2007; Mulert et al., 2010; Rosa et al., 2010). However, this  
9 band limiting approach, is clearly suboptimal when gamma responses that are often reported  
10 in the upper portion of the 30-100 Hz frequency range (Muthukumaraswamy, 2010) have  
11 been related to behaviour and other neuronal measures e.g. GABA concentration  
12 (Muthukumaraswamy et al., 2009). An alternative approach taken by other studies, or in  
13 addition to band-limiting gamma, has been to adopt a sparse fMRI sequence (Leicht et al.,  
14 2016; Mulert et al., 2010; Scheeringa et al., 2011) rather than conventional, continuous fMRI  
15 acquisition. Sparse sequences feature an acquisition time shorter than the repetition time (TR)  
16 of the MRI sequence in order to provide a time window with no MRI gradients present in  
17 which to collect EEG data. As a result this approach enables the full gamma frequency range  
18 to be investigated. However, conventional MRI sequences require a long TR (>3s) and/or  
19 small number of slices to be acquired to provide the required sparsity; imposing limitations in  
20 the temporal sampling or spatial coverage possible and consequently limiting the utility of the  
21 fMRI data acquired.

22  
23  
24 Therefore in order to optimize simultaneous EEG-fMRI recordings to study gamma-BOLD  
25 coupling, we need to establish a novel method to obtain cleaner EEG data in the high  
26 (>30Hz) frequency band. Multiband (MB) fMRI has the potential to overcome the limitations  
27 imposed by conventional sparse fMRI sequences. MB acquisition (Feinberg et al., 2010;  
28 Moeller et al., 2010) can be employed to: shorten repetition times (TR); increase brain  
29 coverage for a given TR; or shorten the acquisition time of whole-head fMRI in a sparse  
30



1  
2  
3 fMRI sequence which would lengthen the gradient-free time window in which EEG data can  
4 be collected. Sparse MB fMRI acquisitions therefore offer great potential for improving EEG  
5 data quality during simultaneous acquisitions. However, due to the additional radio frequency  
6 (RF) power of MB excitation the safety of EEG-MB fMRI acquisitions must be assessed  
7 (Auerbach et al., 2013). In addition, as MB methods can affect temporal signal to noise  
8 (tSNR) of fMRI data (Chen et al., 2015; Todd et al., 2016) assessing the implementation of  
9 MB and the effect on fMRI tSNR is also important to enable optimised EEG-fMRI studies to  
10 take place.

11  
12 Therefore the aim of this work was to assess the overall feasibility of recording EEG  
13 simultaneously with MB fMRI in humans. This took place in three parts: i) assessing the  
14 safety implications of EEG-MB fMRI; ii) assessing the tSNR of MB fMRI and iii) applying  
15 an optimised EEG-MB fMRI approach to investigate single-trial coupling relationships  
16 between MB-BOLD and gamma and beta frequency EEG responses to a finger-abduction  
17 motor task. We chose to investigate motor responses **as an event-related synchronisation**  
18 **(ERS) of gamma oscillations (reflecting an increase in power), typically accompanied by**  
19 **desynchronization (ERD) of beta frequency (15-30Hz) oscillations (reflecting a reduction in**  
20 **power),** in the primary motor cortex contralateral to the movement have been well  
21 documented using invasive electroencephalography (ECoG) (Darvas et al., 2010), MEG  
22 (Muthukumaraswamy, 2010) and EEG (Cheyne et al., 2008) (for reviews, Cheyne and  
23 Ferrari, 2013; Cheyne, 2013; Muthukumaraswamy, 2013). To our knowledge, the motor  
24 gamma-BOLD relationship has not previously been investigated with simultaneous EEG-  
25 fMRI acquisition in humans. Therefore, through this proof of concept study we also aim to  
26 widen the understanding of gamma-BOLD coupling across the cortex. We hypothesise that  
27 the single-trial positive BOLD response in contralateral motor cortex will correlate positively  
28 with **gamma power ERS and negatively with beta power ERD.**

## Methods

Data were acquired and analysed in two stages. Stage one consisted of initial safety testing and image-quality optimisation of EEG-MB fMRI; whilst stage two involved the application of the optimised scanning protocol for the concurrent EEG-fMRI study of human brain responses during motor tasks.

During both stages, EEG data were acquired using BrainAmp MRplus EEG amplifiers (Brain Products, Munich) with 5kHz sampling rate and an MR-compatible 63-channel EEG cap (EasyCap, Herrsching). The hardware band-pass filters were set to a 0.016-250 Hz range, with a roll-off of 30 dB/octave at high frequency. Electrode layout followed the extended international 10-20 system with an additional channel for recording the electrocardiogram (ECG). FCz was used as the reference electrode. A 3T Philips Achieva MRI scanner with a body transmit and 32-channel receiver-array head coil was used for MR data acquisition. The MB implementation for fMRI acquisitions in this study was from Gyrotools, Zurich. MR-EEG scanner clocks were synchronised for all EEG data acquisition (Mullinger et al., 2008b). All data acquisition on humans was performed with approval from the local ethics committee and informed consent was obtained from all subjects involved in this project.

### Stage 1: Assessing the safety and tSNR of EEG-MB fMRI

#### *Safety testing*

Safety testing was performed on a conductive, head shaped phantom with a conductivity of about  $0.5\Omega^{-1}\text{m}^{-1}$  to mimic skin conductivity (Yan et al., 2010). The phantom was left in the scanner room over night to equilibrate to the ambient temperature. The EEG cap was then

1  
2  
3 connected to the phantom using conductive gel (Abralyte 2000 [EasyCap GmbH, Munich])  
4  
5 and all electrode impedances were maintained below 15k $\Omega$ . Fibre-optic thermometers  
6  
7 (Luxtron Corporation, Santa Clara, CA, USA) were used to continually monitor (1 Hz  
8  
9 sampling rate) heating effects at seven locations: four scalp electrodes (Cz, TP7, FCz & TP8),  
10  
11 the ECG lead (connected to the base of the phantom's neck), the cable bundle coming from  
12  
13 the EEG cap and the scanner bore (as a control measurement of heating effects unrelated to  
14  
15 the presence of the EEG system). Thermometer sensors were placed in the conductive gel  
16  
17 under the electrodes and taped to the surface of the cable bundle and scanner bore. The  
18  
19 phantom was then placed at the MR scanner iso-centre. Firstly, a 5-minute recording of  
20  
21 baseline temperature at each location was collected without any scanning. Then two 20-  
22  
23 minute MRI scans, both employing MB factor 4 and **spectral presaturation with inversion**  
24  
25 **recovery (SPIR)** fat suppression, were performed to test for heating during the highest  
26  
27 realistic values of specific absorption rate (SAR) for a given sequence type. **Please note MB**  
28  
29 **factor 4 was the highest available in this implementation of MB.** The sequences tested were:  
30  
31  
32 1) gradient echo (GE)-EPI (using: TR/TE=1000/40ms, SENSE=2, slices=48, B1  
33  
34 RMS=1.09 $\mu$ T, SAR/head=22%); 2) Pseudo-continuous arterial spin labelling (PCASL)-GE-  
35  
36 EPI (using: TR/TE=3500/9.8ms, SENSE=2, slices=32, B1 RMS=1.58 $\mu$ T, SAR/head=46%).  
37  
38 Between the two MRI scans there was a 10 minute period without scanning to allow a return  
39  
40 to baseline following any heating effects from the previous MRI scan.  
41  
42  
43

#### 44 Analysis

45  
46  
47 The mean baseline temperature at each thermometer location was determined using the 5  
48  
49 minute recording prior to each MRI scan. For each location, the mean baseline temperature  
50  
51 was then subtracted from the temperature timeseries recorded during each scan to give the  
52  
53 change in temperature across the whole 20 minute scan period.  
54  
55  
56  
57  
58  
59  
60

### *Image quality: tSNR*

To assess the effect of the implementation of MB excitation on the fMRI signal tSNR, fMRI data were recorded on 3 healthy-adult subjects (age  $32 \pm 2$  years) during five different GE-EPI pulse sequences:

- i) MB factor = 1 with equidistant slice acquisition
- ii) MB factor = 2 with equidistant slice acquisition
- iii) MB factor = 2 with sparse slice acquisition
- iv) MB factor = 3 with equidistant slice acquisition
- v) MB factor = 3 with sparse slice acquisition

Equidistant acquisition used the full TR period, comprised of equal temporal intervals between each slice acquisition. For sparse acquisitions MR data were acquired in the minimum possible time at the beginning of the TR period; the rest of the TR period then formed a quiet period with no MR gradients. A TR = 3060ms and 36 slices were chosen to ensure that these parameters could be used for all combinations of MB factors and slice acquisition (in scans i-v) whilst adhering to requirements for EEG clock synchronisation (Mandelkow et al., 2006; Mullinger et al., 2008b). Other parameters were set for all scans as follows: TE= 40ms, SENSE=2, flip angle=79°, 41 volumes acquired. A T1-weighted anatomical image was also acquired for each subject.

### Analysis

For each subject the anatomical image was used to segment the grey matter (FSL FAST, <https://fsl.fmrib.ox.ac.uk/fsl/>) (Zhang et al., 2001) which formed a mask for subsequent analysis. The tSNR was calculated in every grey matter voxel (Eq. 1) and then averaged over voxels for each subject. The group mean and standard deviation in grey matter of the tSNR

was then found for each of the five scans to assess the change in tSNR with MB factor and slice acquisition scheme.

$$tSNR_{voxel} = \frac{\text{mean signal over time}_{voxel}}{\text{standard deviation over time}_{voxel}}$$

**Eq. 1**

## **Stage 2: EEG-fMRI motor study**

12 right-handed subjects (10 males, 2 females, age = 26.6 ±5.7) took part in the study. After initial data processing, two subjects were excluded from further analysis due to repeated, excessive head motion (>4mm, as assessed from fMRI realignment parameters).

### *Data acquisition*

The EEG cap was put on the subject and all electrode impedances were maintained below 10kΩ for the duration of the study. EEG-fMRI data were acquired using a sparse GE-EPI scheme (TR=3000ms (of which: acquisition time=750ms, quiet period=2250ms), TE=40ms, MB factor=3, 33 slices, voxels=3mm<sup>3</sup>, SENSE = 2, FOV = 240 x 240 mm, flip angle = 79°, 192 volumes, SAR/head<7%). These parameters had been optimised based on the results of Stage 1 and the requirements of the paradigm (see below). High frequency (>30 Hz) artefacts were minimised by mechanically isolating the EEG amplifiers from the scanner bed and minimising MR scanner room environment noise (Mullinger et al., 2013; Mullinger and Bowtell, 2011). In addition, the subject was positioned such that electrodes Fp1 and Fp2 were at the iso-centre in the foot/head direction so as to further reduce the amplitude of the GAs (Mullinger et al., 2011). Foam padding was placed around the subject's head to reduce motion-related artefacts. The EEG and MR scanner clocks were synchronised (**Brain Products Synchbox**), and the TR made equal to a multiple of the EEG sampling period, to ensure consistent sampling of the GA waveforms (Mandelkow et al., 2006; Mullinger et al.,

1  
2  
3 2008b). The onset of every TR period was marked in the EEG data to facilitate GA  
4 correction. Simultaneous electromyogram (EMG) recordings were made from electrodes  
5 attached over the first dorsal interosseous (FDI) muscle of the right hand using a Brain  
6 Product EXG amplifier. Cardiac and respiratory cycles were simultaneously recorded using  
7 the scanner's physiological monitoring system (vector cardiogram (VCG) and respiratory  
8 belt). A T1-weighted anatomical image (MPRAGE sequence) with 1mm isotropic resolution  
9 was also acquired. EEG electrode locations were digitised (Polhemus Fastrak) to facilitate  
10 individualised co-registration of electrode positions with each subject's anatomical image.  
11  
12  
13  
14  
15  
16  
17  
18  
19  
20  
21  
22

### 23 *Paradigm*

24  
25  
26 Subjects performed abduction movements of the right-hand index finger in time with an  
27 auditory cue (1 kHz tones, 50ms duration, 2.5Hz presentation rate) that was delivered to both  
28 ears via headphones, as previously employed in an MEG study (Muthukumaraswamy, 2010).  
29  
30 A single trial consisted of four abduction movements which were performed briskly  
31 following each auditory cue within the MR gradient quiet period of a single TR. The onset of  
32 the first cue was 250ms after the end of the MR acquisition in that TR, such that the cues  
33 occurred at 1000, 1400, 1800 and 2200ms relative to the start of a given TR, resulting in all  
34 movements occurring within a 1.5s window for each trial. Abduction trials were separated by  
35 a 16s (five 3s TR periods + 750ms MR acquisition + 250ms) resting baseline interval (see  
36 Figure 1). Subjects were instructed to fixate on a centrally displayed cross, to keep their  
37 hands by their sides and to remain as still as possible throughout the whole experiment.  
38  
39 Immediately prior to the first auditory cue of each trial, a visual cue appeared, the fixation  
40 cross changed to a plus sign for 2s, warning the subjects to prepare for the upcoming trial.  
41  
42 Subjects performed a 10-minute practice outside the scanner (50 trials of the same auditory  
43  
44  
45  
46  
47  
48  
49  
50  
51  
52  
53  
54  
55  
56  
57  
58  
59  
60

1  
2  
3 **cued abduction task for 1.5s, separated by an interval of 5.5s and EEG recorded)** in order to  
4 familiarize themselves with the paradigm and were then subsequently positioned inside the  
5 MRI scanner where they each completed four runs of 30 trials during fMRI, resulting in 120  
6 trials per subject in total.  
7  
8  
9

## 10 11 Analysis

### 12 *EEG*

13  
14  
15  
16  
17 Cardiac R-peaks were detected from the VCG recording and used to inform pulse artefact  
18 correction of data recording inside the scanner (Mullinger et al., 2008b). For both EEG and  
19 EMG data, gradient and pulse artefacts were corrected in BrainVision Analyzer2 using  
20 sliding window templates formed from the averages of 45 and 21 artefacts respectively,  
21 which were subtracted from each occurrence of the respective artefacts. Data were  
22 subsequently downsampled (600Hz), bandpass filtered (EEG: 0.5-120Hz, EMG: 0.5-45Hz)  
23 and epoched into single-trials from -16s to 2s relative to the onset of the first auditory cue in  
24 each trial (BrainVision Analyzer2). Through visual inspection of the data, noisy EEG  
25 channels and trials that were contaminated with large motion artefacts, substantial EMG  
26 activity during the baseline period, or showed a lack of abduction movement in the EMG  
27 signal, were removed. This resulted in a group mean ( $\pm$ standard error [SE]) of  $84 \pm 2$  trials  
28 remaining for further analysis. Independent component analysis of the EEG data (ICA,  
29 EEGLAB, <https://scn.ucsd.edu/eeglab/>) was then used to remove eye-blinks/movements  
30 (Delorme and Makeig, 2004; Jung et al., 2000), with an average of 2 ICs ( $SE = 1$ ) removed  
31 per subject, and data were re-referenced to an average of all non-noisy channels.  
32  
33  
34  
35  
36  
37  
38  
39  
40  
41  
42  
43  
44  
45  
46  
47  
48  
49

50 Individual, 4-layer (scalp, skull, CSF, & brain) boundary element (BEM) head models were  
51 constructed from the T1 anatomical image of each subject using the Fieldtrip toolbox  
52 (<http://www.ru.nl/neuroimaging/fieldtrip>) (Oostenveld et al., 2011). A Linearly Constrained  
53  
54  
55  
56  
57  
58  
59  
60

1  
2  
3 Minimum Variance (LCMV) beamformer (Robinson and Vrba, 1999; van Dronkelen et al.,  
4 1996; van Veen et al., 1997) was then employed to separately spatially localise changes in  
5 each subject's gamma (55–80Hz) and beta (15-30Hz) frequency oscillations (filtered using  
6  
7 2<sup>nd</sup> order Butterworth filters implemented in Matlab) in response to abduction movements.  
8  
9  
10 The optimal frequency band for the localisation of gamma ERS was determined based on an  
11 iterative process of initially investigating time-frequency spectrograms created from broad  
12 gamma band (30-100Hz) source localisation and observing that consistently, across subjects,  
13 the peak gamma ERS was found in the 55-80Hz, gamma band range, in agreement with many  
14 previous findings (Ball et al., 2008; Cheyne et al., 2008; Muthukumaraswamy, 2010; for  
15 reviews, Cheyne and Ferrari, 2013; Cheyne, 2013; Muthukumaraswamy, 2013). For each  
16 subject and frequency band (beta or gamma), source power during the active (0s to 1.5s) and  
17 passive (-9.0s to -7.5s) time windows, defined relative to the first cue onset, were calculated.  
18 The passive window definition in the baseline interval, during the first MR-quiet period that  
19 preceded the visual probe cue of that trial, was chosen to avoid both the periods of MR  
20 acquisition and any brain activity occurring due to the visual cue. Subsequently, pseudo T-  
21 statistic ( $\mathbb{T}$ -statistic) maps were computed as the ratio of the difference in source power  
22 between the active and passive windows, divided by the sum of the noise power estimates  
23 inherent to the sensors during both active and passive windows (Hillebrand and Barnes, 2005;  
24 Robinson and Vrba, 1999).

25  
26  
27  
28  
29  
30  
31  
32  
33  
34  
35  
36  
37  
38  
39  
40  
41  
42  
43  
44 The maximum peak  $\mathbb{T}$ -statistic location of the gamma power ERS and minimum peak  $\mathbb{T}$ -  
45 statistic location of the beta power ERD in the contralateral primary motor cortex (cM1)  
46 defined the site of a gamma and a beta virtual electrode (VE). A broadband (1-120Hz)  
47 timecourse of neural activity was then extracted from these two VE locations, by multiplying  
48 the channel level data by the respective broadband beamformer weights. Time-frequency  
49 spectrograms of gamma and beta VE data were calculated using a multitaper wavelet  
50  
51  
52  
53  
54  
55  
56  
57  
58  
59  
60



1  
2  
3 approach (Scheeringa et al., 2011). Windows of 0.4s duration were moved across the data in  
4  
5 steps of 50ms, resulting in a frequency resolution of 2.5Hz, and the use of seven tapers  
6  
7 resulted in a spectral smoothing of  $\pm 10$ Hz. Using the mean of the passive window data as  
8  
9 baseline the spectrograms were converted to display change in activity relative to baseline.  
10  
11 Separately for each subject, VE timecourses were filtered into the gamma and beta bands,  
12  
13 Hilbert transformed and then the average power during the active window was calculated for  
14  
15 each trial (Mayhew et al., 2010; Mullinger et al., 2014). These single trial power values were  
16  
17 then mean-subtracted to form regressors of gamma and beta power, which represented the  
18  
19 trial-by-trial variability in single-trial stimulus response amplitudes, for subsequent GLM  
20  
21 analysis of fMRI data. The amplitude of rejected trials was set to the mean value (zero). EEG  
22  
23 data recorded outside the scanner were analysed using equivalent methodology, to provide  
24  
25 comparison of data quality with the inside scanner recordings.  
26  
27  
28  
29  
30  
31

### 32 *fMRI*

33  
34  
35 fMRI data were processed using FSL v5.0.9 (<https://fsl.fmrib.ox.ac.uk/fsl/>). Data from each  
36  
37 subject were corrected for physiological noise using a RETROICOR approach (Glover et al.,  
38  
39 1999) implemented using in-house Matlab code, motion corrected (MCFLIRT), spatially  
40  
41 smoothed (5mm FWHM Gaussian kernel), high-pass temporally filtered (100s cutoff),  
42  
43 registered to their T1 anatomical brain image (FLIRT), and normalised to the MNI 2mm  
44  
45 standard brain. GLM analyses were performed using FEAT v6.0. First-level analysis was  
46  
47 performed employing four regressors: 1) boxcar abduction movement, 2) boxcar visual probe  
48  
49 cue, 3&4) parametric modulation of single-trial gamma and beta neuronal responses,  
50  
51 respectively. All regressors were convolved with the double-gamma HRF. Both positive and  
52  
53 negative contrasts were assessed for each regressor. For each subject and frequency band,  
54  
55  
56  
57  
58  
59  
60

1  
2  
3 first-level results were combined across all four runs using a second-level, fixed effects  
4 analysis to calculate an average response per subject. These results were then combined  
5 across all subjects at the third, group-level using a FLAME mixed-effects analysis (Woolrich  
6 et al., 2004). Since our a-priori hypothesis was to investigate motor fMRI responses and their  
7 correlation with gamma and beta EEG activity, a mask of motor cortex (Oxford–Harvard  
8 cortical atlas, FSL) was applied as pre-threshold mask to all group-level statistical maps  
9 before cluster correction. Main effect (boxcar model of the task) and the single trial EEG  
10 regressor correlation BOLD Z-statistic images were threshold using  $Z > 2.3$  and cluster  
11 corrected significance threshold of  $p < 0.05$ .

## 22 23 24 25 **Results**

### 26 27 **Stage 1: Feasibility testing**

#### 28 29 *Safety testing*

30  
31  
32  
33  
34 The temperature changes measured at all thermometer sensors during the GE-EPI sequence  
35 are plotted in Figure 2. The greatest heating was observed in the ECG channel, which showed  
36 a  $\sim 0.5^{\circ}\text{C}$  increase. This temperature increase occurred gradually over the first 10 minutes and  
37 then stabilised and showed no further change. Nominal heating was observed in the other  
38 channels. The higher SAR of the PCASL sequence resulted in a greater heating effect than  
39 the GE-EPI, again the largest temperature increase was seen in the ECG channel ( $\sim 0.9^{\circ}\text{C}$ )  
40 with increases in other channels (TP8 =  $\sim 0.8^{\circ}\text{C}$ ) also observed (Figure S1). As this GE-EPI  
41 sequence, with parameters chosen to maximise SAR, showed no heating effect close to  $1^{\circ}\text{C}$ ,  
42 the use of the MB GE-EPI (with parameters resulting in lower SAR) with the EEG system  
43 was regarded safe for the following experiments (Carmichael et al., 2008; Medicines and  
44 Healthcare Products Regulatory Agency, 2015).

### *Image quality: tSNR*

The variation in BOLD tSNR with MB factor = 1-3 and slice spacing acquisition is summarised in Table 1. These data indicate that the variability in tSNR between subjects was far larger than the variability of tSNR with imaging parameters. Figure 3 shows the spatial variation in tSNR over a single slice for each subject for the two sparse imaging acquisition sequences tested, which were the most promising sequences for our EEG-fMRI application. Visual inspection of the images in Figure 3 and direct comparison of the mean and standard deviation of tSNR within subjects shows no clear change in tSNR ( $12.6 \pm 22\%$  between MB factor 2 to 3) between MB factors. Since, for sparse sequences, using a MB factor of 3 compared with 2 results in a 33% reduction in the time required to acquire the same number of slices the MB factor of 3 was chosen for the EEG-fMRI experiment, to maximise the duration of the MR quiet-period for EEG measurements without degradation of the tSNR.

### **Study 2: EEG-fMRI motor study**

All subjects performed the abduction task as instructed, judged by visual inspection of the EMG data showing increases in power during brisk finger movements which accurately timed to the auditory cues, and EMG power returning to rest levels during the baseline periods showing subjects remained still in these periods. Mean rectified EMG activity during the passive and active periods is shown for a representative subject in Figure 4.

Figure 5 shows the group average  $F$ -statistic map of changes in both EEG gamma- and beta-power during the active window compared to the passive window. An increase in gamma power (ERS, positive  $F$  values, Fig. 5a) was only observed in contralateral M1, whereas a decrease in beta power (ERD, negative  $F$  values, Fig. 5b) was observed in bilaterally in

1  
2  
3 contralateral and ipsilateral M1. Specifically, the mean of the individual subject VE locations  
4 in cM1 for the gamma ERS was found at:  $[-21\pm3, -31\pm3, 59\pm3]$  mm  $[MNI:x,y,z]$  (see Fig 5a,  
5 crosshair) and the beta ERD was found at  $[-39\pm3, -32\pm2, 51\pm4]$  mm (see Fig 5b, crosshair),  
6 where errors denote standard error over subjects. Both these locations lie in the post-central  
7 gyrus, the gamma VE location was found to be significantly more medial ( $t(9) = 3.76$ ,  
8  $p=0.004$  paired t-test) than the beta VE location, but no difference in the y ( $t(9) = 0.41$ ,  
9  $p=0.69$ ) or z ( $t(9) = 1.32$ ,  $p=0.21$ ) co-ordinates was observed.  
10  
11  
12  
13  
14  
15  
16  
17

18 Figure 6 shows the group mean time-frequency spectrograms measured from cM1 for the  
19 gamma (Fig 6a&b) and beta (Fig 6c&d) VE locations. Figures 6a&c display the mean time-  
20 frequency spectrogram for the whole 18s duration of the abduction trial and preceding inter-  
21 trial interval, with Figure 6b&d showing the active and passive periods only. The broadband  
22 increases in power (red vertical stripes lasting  $\sim 750$ ms and occurring every 3s) show the  
23 effect of the residual GAs caused by the MRI data acquisition on the EEG power spectrum. It  
24 is clear that neuronal EEG responses above 20 Hz recorded during MRI data acquisition are  
25 corrupted by residual GAs with signal degradation increasing with increasing frequency (Fig.  
26 6a&c). Note that, due to the way the trials were epoched, the increase in  $<30$ Hz power  
27 between -16s and -14s represents the post-movement alpha/beta rebound. By selecting the  
28 active (0 to 1.5s) and passive (-9 to -7.5s) time windows during MR quiet periods a reliable  
29 comparison of neuronal signals between rest and task was made for both the gamma and beta  
30 bands (Fig. 6b&d). During the active window, when the FDI abduction movements were  
31 performed, **ERS of gamma band power (55-80Hz) and ERD of beta band power (15-30Hz)**  
32 occurred compared with the passive window of baseline resting fixation with no movement  
33 (Fig. 6b&d). As expected due to the VE definition, stronger **gamma power ERS was observed**  
34 **in the gamma VE than the beta VE, and stronger beta power ERD** was observed in the beta  
35 VE than in the gamma VE. **Comparison of these results with those from data recorded outside**  
36  
37  
38  
39  
40  
41  
42  
43  
44  
45  
46  
47  
48  
49  
50  
51  
52  
53  
54  
55  
56  
57  
58  
59  
60

the scanner (Figure S2 & S3), show that very similar gamma and beta responses were measured in both recordings, providing confidence in the quality of our data inside the scanner.

As expected across 10 subjects, we observed a significant main-effect (correlation with boxcar regressor) positive BOLD response to the abduction movements in the motor cortex, with the peak voxel ( $Z=5.12$ ,  $p<1\times 10^{-19}$ ) lying within the masked region found at  $[-38, -32, 66]$  mm  $[MNI:x,y,z]$  in cM1, as shown in Figure 7, red-orange. With a second peak ( $Z=4.97$ ,  $p<1\times 10^{-19}$ ) found on the midline at  $[-4, -14, 70]$  mm  $[MNI:x,y,z]$ . In addition a positive correlation between single-trial gamma power ERS and the BOLD response was observed in cM1, with the peak ( $Z=3.11$ ,  $p<0.001$ ) located at  $[-32, -42, 60]$  mm  $[MNI:x,y,z]$  (Fig 7, green) with additional responses in the ipsilateral primary motor cortex with the peak ( $Z=3.02$ ,  $p<0.01$ ) located at  $[34, -42, 60]$  mm  $[MNI:x,y,z]$  and on the midline with peak ( $Z=2.97$ ,  $p<0.01$ ) located at  $[2, -36, 56]$  mm  $[MNI:x,y,z]$ . No significant negative correlations were observed with the boxcar or gamma band regressors. No significant positive or negative correlations between single-trial beta and BOLD responses were observed.

## Discussion

Here, through a series of experiments we show that, with the right safety precautions and MRI sequence choice, it is safe to simultaneously acquire EEG data with MB fMRI data, despite the higher peak RF power required for MB acquisitions compared with conventional fMRI acquisitions. We also show that, for the implementation of MB used here, there is no measurable degradation of the fMRI signal tSNR when moving to a sparse acquisition with a MB factor of 3 compared with the conventional continuous equi-spacing acquisition with no MB factor, allowing for the presence of physiological noise. We finally show the

1  
2  
3 considerable gains that can be achieved in using MB fMRI with concurrent EEG data  
4 acquisition by studying gamma-BOLD coupling with a simple motor task. We were able to  
5 reliably detect the gamma response to finger abductions within cM1 and found that this  
6 response was positively correlated with the BOLD response in bilateral primary motor cortex  
7 with activation extending directly posterior to the hand-knob area of the contralateral motor  
8 cortex.  
9  
10  
11  
12  
13  
14  
15  
16  
17  
18

### 19 *Safety and signal quality considerations*

20  
21 We show that for a GE-EPI sequence using a MB factor of 4 resulting in a B1 RMS=1.09 $\mu$ T,  
22 SAR/head=22% that the maximum heating observed over a 20 minute period was  $\sim$ 0.5 $^{\circ}$ C  
23 (Figure 2) which is considerably less than the recommended 1 $^{\circ}$ C safety limit (Medicines and  
24 Healthcare Products Regulatory Agency, 2015). Furthermore the majority of this 0.5 $^{\circ}$ C  
25 temperature increase was observed within the first 5-6 minutes of scanning after which the  
26 temperature remained relatively constant suggesting that there is not a linear heating effect  
27 over time. Therefore even if data were continuously acquired for a longer period, which is  
28 uncommon in neuroimaging studies, the risk to the subject is unlikely to increase greatly. A  
29 similar pattern of heating was observed for the PCASL sequence where the greatest heating  
30 occurred in the first few minutes before a plateau was reached (Figure S1). However, this  
31 heating effect was far greater, up to  $\sim$ 0.9 $^{\circ}$ C over the electrodes and locations measured,  
32 reflecting the increased B1 power used in that sequence (B1 RMS=1.58 $\mu$ T, SAR/head=46%).  
33 As this temperature rise was only just within the safe limit for human tissue (Medicines and  
34 Healthcare Products Regulatory Agency, 2015) and given that not all locations on the  
35 phantom were monitored, we would strongly suggest sequences such as MB-PCASL should  
36 not be used with concurrent EEG recordings. **Although we didn't record temperature data**  
37  
38  
39  
40  
41  
42  
43  
44  
45  
46  
47  
48  
49  
50  
51  
52  
53  
54  
55  
56  
57  
58  
59  
60

1  
2  
3 from occipital electrodes due to practical limitations, we believe temperature increases at  
4  
5 T7/T8 are likely to approximate the O1/O2 electrodes, due to similar wire lengths. The  
6  
7 greatest heating effect in both GE-EPI and PCASL scans was observed in the ECG lead. This  
8  
9 lead is considerably longer than the other leads in the EEG cap, which probably resulted in  
10  
11 greater RF absorption in this lead (Mullinger et al., 2008a) causing the larger heating effect  
12  
13 observed here. Given the potential to use the VCG system, supplied by the MRI  
14  
15 manufacturer, to monitor the cardiac cycle (Mullinger et al., 2008b) it would be possible to  
16  
17 reduce the risk of heating effects by removing the ECG lead and electrode from the EEG  
18  
19 setup. However, given the increase in temperature ( $\sim 0.8$  °C) in the Tp8 electrode, which also  
20  
21 has a relatively long lead, the removal of the ECG lead alone is unlikely to ensure that high  
22  
23 SAR sequences can be run safely with EEG system present. These findings are in general  
24  
25 agreement with recent work that also considered safety implication of MB (Foged et al.,  
26  
27 2017). It is also important to note that minimal heating effects were observed at the MRI  
28  
29 scanner bore location suggesting that the MR scanning was not increasing the ambient  
30  
31 temperature of the bore. Therefore the observed electrode heating specifically arose from the  
32  
33 interaction between the EEG system and the RF slice excitation pulses. These data highlight  
34  
35 the potential dangers of using MB sequences for EEG-fMRI where high SAR values can arise  
36  
37 from the increased B1 (Collins and Wang, 2011) and the need for specific safety testing of  
38  
39 any sequences used. Since there are choices in how the RF pulses required for MB sequences  
40  
41 can be implemented, with varying effects on SAR (Feinberg and Setsompop, 2013; Norris et  
42  
43 al., 2011; Wong, 2012), it is important that MB implementations by different MR  
44  
45 manufactures and software providers are individually tested before being used in human  
46  
47 experiments.  
48  
49  
50  
51  
52  
53  
54  
55  
56  
57  
58  
59  
60

1  
2  
3 It is known that the use of MB can reduce image quality and consequently degrade the  
4 temporal stability of the signals acquired using EPI based sequences (Chen et al., 2015; Todd  
5 et al., 2016). However, due to the ability of MB to shorten the TR, the increased temporal  
6 sampling can result in increased signal sensitivity per unit time as well as enhanced t-  
7 statistics of activation maps (Todd et al., 2016). MB fMRI has been shown to be useful in a  
8 number of different applications since its conception only a few years ago, with the relative  
9 gains in sampling rate and voxel size that it can provide offsetting any signal quality  
10 degradation incurred (Boyacıoğlu et al., 2015; Feinberg et al., 2010; Moeller et al., 2010;  
11 Olafsson et al., 2015). Indeed, our own investigations showed that the variation in tSNR over  
12 subjects was far greater than the variation in tSNR between the sequences tested with  
13 different MB factors and slice acquisition schemes (Table 1). This suggests that the tSNR  
14 measures were dominated by physiological noise and anatomical variability rather than  
15 imaging sequence differences. Even when changes in tSNR within subjects between MB 2  
16 and 3 were considered there no clear reduction was seen with increasing MB factor (Figure 3)  
17 in these data. By using MB factor = 3 with sparse slice acquisition we were able to maintain  
18 whole-head coverage whilst obtaining a 2.25s MR quiet period, within our 3s TR, in which to  
19 study EEG-BOLD coupling. Therefore the relative gain in quiet period time far outweighed  
20 effects on tSNR which were encountered.  
21  
22  
23  
24  
25  
26  
27  
28  
29  
30  
31  
32  
33  
34  
35  
36  
37  
38  
39  
40  
41  
42  
43  
44

#### 45 *Benefits of MB fMRI for the simultaneous recording of high frequency EEG signals*

46  
47 The presence of residual GAs in EEG data at frequencies above 20 Hz shows the necessity of  
48 an MR quiet period to provide the best SNR for studying beta and gamma band signals.  
49 These residual artefacts are present despite strict adherence to best-current practice  
50 acquisition and the implementation of hardware solutions (synchronisation (Mandelkow et  
51  
52  
53  
54  
55  
56  
57  
58  
59  
60



1  
2  
3 al., 2006; Mullinger et al., 2008) and optimal positioning (Mullinger et al., 2011)) and  
4  
5 beamforming post-processing (Brookes et al., 2009, 2008) which are all designed to minimise  
6  
7 the residual GAs. Whilst the magnitude of the residual GA appears to increase with  
8  
9 frequency (Figure 6), it is actually relatively constant across the frequency bands above 20  
10  
11 Hz (Figure S4c&d), but the relative contribution of the GA to the overall signal is increased  
12  
13 due to the decrease in the amplitude of the underlying neuronal activity at higher frequencies  
14  
15 resulting in Figure S4e&f. These residual artefacts are likely to be caused by sub-millimetre  
16  
17 movements of the subject's head during data acquisition causing small changes in the GA  
18  
19 profile, preventing perfect correction by template subtraction methods (Ritter et al., 2007;  
20  
21 Yan et al., 2009). Given that such small head movements cannot be eliminated during  
22  
23 acquisition and the current lack of a post-processing method to completely remove residual  
24  
25 GAs from the EEG data, despite considerable effort by a number of groups (Brookes et al.,  
26  
27 2008; Freyer et al., 2009; Maziero et al., 2016; Moosmann et al., 2009), the merit of an MR  
28  
29 quiet period, that enables the study of higher frequency neuronal activity unadulterated by  
30  
31 concurrent fMRI acquisition, is clear.  
32  
33  
34  
35  
36  
37  
38

39 Indeed, using a sparse MR sequence incorporating quiet periods has previously been  
40  
41 implemented to allow the study of gamma band activity during fMRI (Leicht et al., 2016;  
42  
43 Mulert et al., 2010; Scheeringa et al., 2011). We have extended these previous works by  
44  
45 showing that beta and gamma band activity from motor cortex can be measured in the MRI  
46  
47 environment. We observed an ERS of gamma band power during the abduction movements  
48  
49 compared with rest (Figs 5a and 6a&b) localised to cM1, in close agreement with previous  
50  
51 MEG studies (Ball et al., 2008; Cheyne, 2013; Darvas et al., 2010; Muthukumaraswamy,  
52  
53 2010). This gamma band response was accompanied by a decrease (ERD) in beta band power  
54  
55 (Figs 5b and 6c&d) which was observed in bilateral M1, in agreement with previous studies  
56  
57  
58  
59  
60

1  
2  
3 collected outside an MRI environment (Darvas et al., 2013; Jurkiewicz et al., 2006;  
4 Muthukumaraswamy et al., 2010). Interestingly, previous invasive and non-invasive  
5 electrophysiological recordings have shown that the gamma ERS is more spatially focal to  
6 cM1 than the beta ERD (Darvas et al., 2013; Miller et al., 2007), which was also observed in  
7 our data. In addition to the difference in the spatial localisation of the gamma/beta responses,  
8 we also observed different temporal profiles between the spectral responses from these  
9 locations. The gamma ERS covered a relatively large frequency range (~50-80Hz) and,  
10 whilst it could be seen for the entire movement period, it was strongest at initial movement  
11 onset (i.e. 0-0.5s Fig 6a). The beta ERD was found to be much stronger and was present  
12 consistently throughout the entire movement period. Together these differences in spatial  
13 location and temporal response profile suggest different neuronal populations are driving  
14 these two responses, in line with previous findings (Darvas et al., 2010; Miller et al., 2007).  
15  
16  
17  
18  
19  
20  
21  
22  
23  
24  
25  
26  
27  
28  
29  
30  
31

32 Given the considerable advantages of MRI for providing excellent spatial resolution of brain  
33 activity (De Martino et al., 2015; Heidemann et al., 2012) it is highly desirable to take  
34 advantage of this feature in the investigation of the origin of electrophysiological responses,  
35 where non-invasive EEG/MEG recordings are limited. However, previous studies (Leicht et  
36 al., 2016; Mulert et al., 2010; Scheeringa et al., 2011) have required considerable  
37 compromise on spatial resolution (slice thickness ranging from 4-8mm with slice gaps of 0.4-  
38 1mm) and/or brain coverage (between 35 and 120mm) to provide a sufficient quiet period to  
39 TR ratio (ranging between 30-90% of time) and sampling rate of MRI responses (TRs  
40 between 3 and 3.63s). With the current implementation of MB we have shown that these  
41 trade-offs can be minimised such that 3 mm isotropic voxels, with no slice gap and 99 mm  
42 brain coverage with a quiet period to TR ratio of 75%, can be achieved with a TR of 3s.  
43  
44  
45  
46  
47  
48  
49  
50  
51  
52  
53  
54  
55  
56  
57  
58  
59  
60

*BOLD responses and coupling to EEG responses and future research possibilities*

Exploiting the advantages of EEG-MB fMRI has allowed us to show the potential of this technique for non-invasively investigating brain function. We found that, out of all our regressors, the boxcar model of the finger abductions showed the strongest correlation with the BOLD response, with the largest activations arising in the contralateral postcentral gyrus (M1) [-38, -32, 66] mm, and supplementary motor area [-4, -14, 70] mm as well as bilateral S2. All of which are regions expected to be activated in a simple sensorimotor task. Interestingly the regions of gamma-BOLD correlation were smaller and more focal, with peak activity being observed between the postcentral gyrus and superior parietal lobule both in contralateral [-32,-42, 60] mm, ipsilateral [34, -42, 60] mm regions, and a central peak found between precentral and postcentral gyrus at [2, -36, 56] mm. The contralateral activation extends to directly posterior to the hand-knob area of the left sensorimotor cortex, further suggesting this was a localised, task specific response. The bilaterality of this correlation, given the gamma ERS was lateralised to the left cM1, appears surprising, but falls consistently within the bilateral somatosensory cortex and therefore is likely to arise due to the mutual correlation of BOLD signals between the contralateral and ipsilateral regions of the somatosensory network for this task.

It is unsurprising given the robust task employed that the BOLD response was well characterised by a simple boxcar model and that this showed the strongest activations in the motor network. However, single-trial variability in BOLD and gamma ERS response amplitudes were well coupled in the somatosensory network. This finding supports previous work showing a tight coupling of natural variability in BOLD and gamma responses in the visual system (Logothetis, 2003; Scheeringa et al., 2011) and extends these findings into the

1  
2  
3 sensorimotor modality. It is likely that the BOLD-gamma coupling was most evident in the  
4  
5 sensory network where the variability to the task was the greatest and therefore least  
6  
7 explained by the boxcar constant main effect. We hypothesize that a greater amount of  
8  
9 response variability was elicited in the somatosensory network than the motor cortex as the  
10  
11 subject's abduction movements showed such a high level of consistency in both timing and  
12  
13 amplitude (Fig 4), reflecting similar motor output. However, it is possible that the sensation  
14  
15 of finger movement, and thus the somatosensory input, may have varied depending on what  
16  
17 external surfaces were touched with the finger when subjects' arms were slightly cramped for  
18  
19 space inside the scanner. Whilst this cannot be proven with these data, it provides a basis for  
20  
21 further investigation.  
22  
23

24  
25  
26  
27  
28 The lack of significant correlation between the beta ERD and BOLD responses appears a  
29  
30 surprising result given previous reports of negative beta-BOLD correlations (Ritter et al.,  
31  
32 2009) and the clear beta band responses which we observed (Fig 5b). However, here we  
33  
34 considered the variability in the EEG response which explained variance in the BOLD data in  
35  
36 addition to that explained by a constant amplitude boxcar model. Further inspection of our  
37  
38 data with a fixed effects cluster corrected  $Z > 2.0$  group analysis showed that beta-BOLD  
39  
40 correlations were observed in central and ipsilateral motor cortex, but these did not survive  
41  
42 mixed effects  $Z > 2.3$ . Therefore it seems that the effect size was too weak for the beta  
43  
44 correlation to arise in our data sample. Beta ERD is widely observed during preparation and  
45  
46 execution of movements (Engel and Fries, 2010; Ritter et al., 2009; Zaepffel et al., 2013),  
47  
48 however there is a sparsity of evidence directly linking parameters of the beta ERD amplitude  
49  
50 to the quality of motor performance, leaving much still to be understood concerning beta  
51  
52 oscillations precise functional role (Engel and Fries, 2010; Kilavik et al., 2013; Pogosyan et  
53  
54 al., 2009). Given the beta ERD has been considered to be a simple gating mechanism (Fry et  
55  
56  
57  
58  
59  
60

1  
2  
3 al., 2016; Stevenson et al., 2011) required to allow neuronal activity involved in task  
4  
5 execution to take place in other, typically higher, frequency bands it is conceivable that the  
6  
7 amplitude variability of the ERD is less related to the task performance and reflects more of a  
8  
9 binarised signal to permit the necessary activation.  
10

11  
12  
13  
14  
15 In conclusion we show that EEG can be safely acquired concurrently with GE-EPI MB-fMRI  
16  
17 data and allows the investigation of neuronal and hemodynamic task responses with high  
18  
19 spatial, temporal and spectral resolution. We use a simple motor task in this work to show  
20  
21 that tight gamma-BOLD coupling is observed on an individual trial basis, agreeing with  
22  
23 previous invasive recordings in both animal and human visual/auditory cortex. In the future  
24  
25 such methodologies that allow detailed integration of a wide frequency range of neural  
26  
27 signals may be used to build a more complete understanding of pathways of feedforward and  
28  
29 feedback neural communication and of how such signals contribute to neurovascular  
30  
31 coupling mechanisms and the generation of the hemodynamic response.  
32  
33  
34  
35  
36  
37

### 38 **Acknowledgements**

39  
40 We thank the Birmingham Nottingham Strategic Collaboration Fund for supporting this work  
41  
42 and MU and a University of Nottingham Anne McLaren Fellowship for funding KJM and a  
43  
44 University of Birmingham Fellowship for funding SDM.  
45  
46  
47  
48  
49

### 50 **References**

51  
52  
53 Auerbach, E.J., Xu, J., Yacoub, E., Moeller, S., Ugurbil, K., 2013. Multiband accelerated  
54  
55 spin-echo echo planar imaging with reduced peak RF power using time-shifted RF  
56  
57  
58  
59  
60

- 1  
2  
3 pulses. *Magn Reson Med* 69, 1261–1267. doi:10.1002/mrm.24719  
4  
5  
6 Bagshaw, A.P., Aghakhani, Y., Bénar, C.G., Kobayashi, E., Hawco, C., Dubeau, F., Pike,  
7  
8 G.B., Gotman, J., 2004. EEG-fMRI of focal epileptic spikes: Analysis with multiple  
9  
10 haemodynamic functions and comparison with gadolinium-enhanced MR angiograms.  
11  
12 *Hum. Brain Mapp.* 22, 179–192. doi:10.1002/hbm.20024  
13  
14  
15 Ball, T., Demandt, E., Mutschler, I., Neitzel, E., Mehring, C., Vogt, K., Aertsen, A., Schulze-  
16  
17 Bonhage, A., 2008. Movement related activity in the high gamma range of the human  
18  
19 EEG. *Neuroimage* 41, 302–310. doi:10.1016/j.neuroimage.2008.02.032  
20  
21  
22 Bauer, M., Oostenveld, R., Peeters, M., Fries, P., 2006. Tactile spatial attention enhances  
23  
24 gamma-band activity in somatosensory cortex and reduces low-frequency activity in  
25  
26 parieto-occipital areas. *J Neurosci* 26, 490–501. doi:10.1523/JNEUROSCI.5228-  
27  
28 04.2006  
29  
30  
31 Becker, R., Reinacher, M., Freyer, F., Villringer, A., Ritter, P., 2011. How Ongoing Neuronal  
32  
33 Oscillations Account for Evoked fMRI Variability. *J. Neurosci.* 31, 11016–11027.  
34  
35 doi:10.1523/jneurosci.0210-11.2011  
36  
37  
38 Bénar, C.G., Schön, D., Grimault, S., Nazarian, B., Burle, B., Roth, M., Badier, J.M.,  
39  
40 Marquis, P., Liegeois-Chauvel, C., Anton, J.L., 2007. Single-trial analysis of oddball  
41  
42 event-related potentials in simultaneous EEG-fMRI. *Hum. Brain Mapp.* 28, 602–613.  
43  
44 doi:10.1002/hbm.20289  
45  
46  
47  
48 Boorman, L., Harris, S., Bruyns-Haylett, M., Kennerley, A., Zheng, Y., Martin, C., Jones, M.,  
49  
50 Redgrave, P., Berwick, J., 2015. Long-Latency Reductions in Gamma Power Predict  
51  
52 Hemodynamic Changes That Underlie the Negative BOLD Signal. *J. Neurosci.* 35,  
53  
54 4641–4656. doi:10.1523/JNEUROSCI.2339-14.2015  
55  
56  
57  
58  
59  
60

- 1  
2  
3 Boyacıoğlu, R., Schulz, J., Koopmans, P.J., Barth, M., Norris, D.G., 2015. Improved  
4  
5 sensitivity and specificity for resting state and task fMRI with multiband multi-echo EPI  
6  
7 compared to multi-echo EPI at 7T. *Neuroimage* 119, 352–361.  
8  
9 doi:10.1016/j.neuroimage.2015.06.089  
10  
11
- 12 Brookes, M.J., Mullinger, K.J., Stevenson, C.M., Morris, P.G., Bowtell, R., 2008.  
13  
14 Simultaneous EEG source localisation and artifact rejection during concurrent fMRI by  
15  
16 means of spatial filtering. *Neuroimage* 40, 1090–1104.  
17  
18 doi:10.1016/j.neuroimage.2007.12.030  
19  
20
- 21 Brookes, M.J., Vrba, J., Mullinger, K.J., Geirsdottir, G.B., Yan, W.X., Stevenson, C.M.,  
22  
23 Bowtell, R., Morris, P.G., 2009. Source localisation in concurrent EEG/fMRI:  
24  
25 applications at 7T. *Neuroimage* 45, 440–452. doi:S1053-8119(08)01160-9 [pii]  
26  
27 10.1016/j.neuroimage.2008.10.047  
28  
29
- 30 Brown, P., Salenius, S., Rothwell, J.C., Hari, R., 1998. Cortical correlate of the piper rhythm  
31  
32 in humans. *J. Neurophysiol.* 80, 2911–2917.  
33  
34
- 35 Buschman, T.J., Miller, E.K., 2007. Top-down versus bottom-up control of attention in the  
36  
37 prefrontal and posterior parietal cortices. *Science* 315, 1860–1862.  
38  
39 doi:10.1126/science.1138071  
40  
41
- 42 Buzsaki, G., Draguhn, A., 2004. Neuronal Oscillations in Cortical Networks. *Science* (80-. ).  
43  
44 304, 1926–1929. doi:10.1126/science.1099745  
45  
46
- 47 Carmichael, D.W., Thornton, J.S., Rodionov, R., Thornton, R., McEvoy, A., Allen, P.J.,  
48  
49 Lemieux, L., 2008. Safety of localizing epilepsy monitoring intracranial  
50  
51 electroencephalograph electrodes using MRI: Radiofrequency-induced heating. *J. Magn.*  
52  
53 *Reson. Imaging* 28, 1233–1244. doi:10.1002/jmri.21583  
54  
55  
56  
57  
58  
59  
60

- 1  
2  
3 Castelhano, J., Duarte, I.C., Wibral, M., Rodriguez, E., Castelo-Branco, M., 2014. The dual  
4  
5 facet of gamma oscillations: Separate visual and decision making circuits as revealed by  
6  
7 simultaneous EEG/fMRI. *Hum. Brain Mapp.* 35, 5219–5235. doi:10.1002/hbm.22545  
8  
9
- 10 Chen, L., Vu, A.T., Xu, J., Moeller, S., Ugurbil, K., Yacoub, E., Feinberg, D.A., 2015.  
11  
12 Evaluation of highly accelerated simultaneous multi-slice EPI for fMRI. *Neuroimage*  
13  
14 104, 452–459. doi:10.1016/j.neuroimage.2014.10.027  
15  
16
- 17 Cheyne, D., Bells, S., Ferrari, P., Gaetz, W., Bostan, A.C., 2008. Self-paced movements  
18  
19 induce high-frequency gamma oscillations in primary motor cortex. *Neuroimage* 42,  
20  
21 332–342. doi:10.1016/j.neuroimage.2008.04.178  
22  
23
- 24 Cheyne, D., Ferrari, P., 2013. MEG studies of motor cortex gamma oscillations: evidence for  
25  
26 a gamma “fingerprint” in the brain? *Front. Hum. Neurosci.* 7, 1–7.  
27  
28 doi:10.3389/fnhum.2013.00575  
29  
30
- 31 Cheyne, D.O., 2013. MEG studies of sensorimotor rhythms: A review. *Exp. Neurol.*  
32  
33 doi:10.1016/j.expneurol.2012.08.030  
34  
35
- 36 Colgin, L.L., Denninger, T., Fyhn, M., Hafting, T., Bonnevie, T., Jensen, O., Moser, M.-B.,  
37  
38 Moser, E.I., 2009. Frequency of gamma oscillations routes flow of information in the  
39  
40 hippocampus. *Nature* 462, 353–357. doi:10.1038/nature08573  
41  
42
- 43 Collins, C.M., Wang, Z., 2011. Calculation of radiofrequency electromagnetic fields and their  
44  
45 effects in MRI of human subjects. *Magn. Reson. Med.* 65, 1470–1482.  
46  
47 doi:10.1002/mrm.22845  
48  
49
- 50 Crone, N.E., Miglioretti, D.L., Gordon, B., Lesser, R.P., 1998. Functional mapping of human  
51  
52 sensorimotor cortex with electrocorticographic spectral analysis II. Event-related  
53  
54 synchronization in the gamma band. *Brain* 121, 2301–2315.  
55  
56  
57  
58  
59  
60



1  
2  
3 doi:10.1093/brain/121.12.2301  
4

5 Darvas, F., Rao, R.P.N., Murias, M., 2013. Localized high gamma motor oscillations respond  
6 to perceived biologic motion. *J. Clin. Neurophysiol.* 30, 299–307.  
7

8  
9 doi:10.1097/WNP.0b013e3182872f40  
10

11  
12 Darvas, F., Scherer, R., Ojemann, J.G., Rao, R.P., Miller, K.J., Sorensen, L.B., 2010. High  
13 gamma mapping using EEG. *Neuroimage* 49, 930–938.  
14

15  
16 doi:10.1016/j.neuroimage.2009.08.041  
17

18  
19 De Martino, F., Moerel, M., Xu, J., Van De Moortele, P.F., Ugurbil, K., Goebel, R., Yacoub,  
20 E., Formisano, E., 2015. High-resolution mapping of myeloarchitecture in vivo:  
21 Localization of auditory areas in the human brain. *Cereb. Cortex* 25, 3394–3405.  
22

23  
24 doi:10.1093/cercor/bhu150  
25

26  
27 Debener, S., Ullsperger, M., Siegel, M., Engel, A.K., 2006. Single-trial EEG-fMRI reveals  
28 the dynamics of cognitive function. *Trends Cogn. Sci.* 10, 558–563.  
29

30  
31 doi:10.1016/j.tics.2006.09.010  
32

33  
34 Debener, S., Ullsperger, M., Siegel, M., Fiehler, K., von Cramon, D.Y., Engel, A.K., 2005.  
35

36 Trial-by-trial coupling of concurrent electroencephalogram and functional magnetic  
37 resonance imaging identifies the dynamics of performance monitoring. *J Neurosci* 25,  
38

39  
40 11730–11737. doi:10.1523/JNEUROSCI.3286-05.2005  
41

42  
43 Delorme, A., Makeig, S., 2004. EEGLAB: an open source toolbox for analysis of single-trial  
44

45 EEG dynamics including independent component analysis. *J Neurosci Methods* 134, 9–  
46  
47 21. doi:10.1016/j.jneumeth.2003.10.009 S0165027003003479 [pii]  
48

49  
50 Eichele, T., Calhoun, V.D., Moosmann, M., Specht, K., Jongsma, M.L.A., Quiroga, R.Q.,  
51

52  
53 Nordby, H., Hugdahl, K., 2008. Unmixing concurrent EEG-fMRI with parallel  
54

1  
2  
3 independent component analysis. *Int. J. Psychophysiol.* 67, 222–234.

4  
5 doi:10.1016/j.ijpsycho.2007.04.010

6  
7 Eichele, T., Specht, K., Moosmann, M., Jongsma, M.L.A., Quiroga, R.Q., Nordby, H.,  
8  
9 Hugdahl, K., 2005. Assessing the spatiotemporal evolution of neuronal activation with  
10  
11 single-trial event-related potentials and functional MRI. *Proc Natl Acad Sci U S A* 102,  
12  
13 17798–17803. doi:10.1073/pnas.0505508102

14  
15  
16  
17 Engel, A.K., Fries, P., 2010. Beta-band oscillations-signalling the status quo? *Curr. Opin.*  
18  
19 *Neurobiol.* doi:10.1016/j.conb.2010.02.015

20  
21  
22 Feinberg, D.A., Moeller, S., Smith, S.M., Auerbach, E., Ramanna, S., Gunther, M., Glasser,  
23  
24 M.F., Miller, K.L., Ugurbil, K., Yacoub, E., 2010. Multiplexed echo planar imaging for  
25  
26 sub-second whole brain fMRI and fast diffusion imaging. *PLoS One* 5, e15710.  
27  
28 doi:10.1371/journal.pone.0015710

29  
30  
31 Feinberg, D.A., Setsompop, K., 2013. Ultra-fast MRI of the human brain with simultaneous  
32  
33 multi-slice imaging. *J. Magn. Reson.* doi:10.1016/j.jmr.2013.02.002

34  
35  
36 Fell, J., Klaver, P., Lehnertz, K., Grunwald, T., Schaller, C., Elger, C.E., Fernandez, G.,  
37  
38 2001. Human memory formation is accompanied by rhinal-hippocampal coupling and  
39  
40 decoupling. *Nat. Neurosci.* 4, 1259–1264. doi:10.1038/nn759

41  
42  
43 Foged, M.T., Lindberg, U., Vakamudi, K., Larsson, H.B.W., Pinborg, L.H., Kjær, T.W.,  
44  
45 Fabricius, M., Svarer, C., Ozenne, B., Thomsen, C., Beniczky, S., Paulson, O.B., Posse,  
46  
47 S., 2017. Safety and EEG data quality of concurrent high-density EEG and high-speed  
48  
49 fMRI at 3 Tesla. *PLoS One* 12. doi:10.1371/journal.pone.0178409

50  
51  
52 Freyer, F., Becker, R., Anami, K., Curio, G., Villringer, A., Ritter, P., 2009. Ultrahigh-  
53  
54 frequency EEG during fMRI: Pushing the limits of imaging-artifact correction.

1  
2  
3 Neuroimage 48, 94–108. doi:10.1016/j.neuroimage.2009.06.022  
4

5 Fries, P., 2009. Neuronal gamma-band synchronization as a fundamental process in cortical  
6 computation. *Annu Rev Neurosci* 32, 209–224.  
7

8  
9 doi:10.1146/annurev.neuro.051508.135603  
10

11  
12 Fry, A., Mullinger, K.J., O'Neill, G.C., Barratt, E.L., Morris, P.G., Bauer, M., Folland, J.P.,  
13 Brookes, M.J., 2016. Modulation of post-movement beta rebound by contraction force  
14 and rate of force development. *Hum. Brain Mapp.* 37, 2493–2511.  
15  
16

17  
18 doi:10.1002/hbm.23189  
19

20  
21 Gaetz, W., MacDonald, M., Cheyne, D., Snead, O.C., 2010. Neuromagnetic imaging of  
22 movement-related cortical oscillations in children and adults: Age predicts post-  
23 movement beta rebound. *Neuroimage* 51, 792–807.  
24  
25

26  
27 doi:10.1016/j.neuroimage.2010.01.077  
28

29  
30 Glover, G.H., Li, T.Q., Ress, D., 1999. Image-based method for retrospective correction of  
31 physiological motion effects in fMRI: RETROICOR. *Magn Res Med* 44 (1) 162-167.  
32  
33

34  
35 doi:10.1002/mrm.1522-2594(200007)44  
36

37  
38 Goldman, R.I., Stern, J.M., Engel Jerome, J., Cohen, M.S., 2002. Simultaneous EEG and  
39 fMRI of the alpha rhythm. *Neuroreport* 13, 2487–2492.  
40  
41

42  
43 doi:10.1097/01.wnr.0000047685.08940.d0  
44

45 Goldman, R.I., Wei, C.Y., Philiastides, M.G., Gerson, A.D., Friedman, D., Brown, T.R.,  
46 Sajda, P., 2009. Single-trial discrimination for integrating simultaneous EEG and fMRI:  
47 identifying cortical areas contributing to trial-to-trial variability in the auditory oddball  
48 task. *Neuroimage* 47, 136–147. doi:10.1016/j.neuroimage.2009.03.062  
49  
50  
51  
52

53  
54 Green, J.J., Boehler, C.N., Roberts, K.C., Chen, L.-C., Krebs, R.M., Song, A.W., Woldorff,  
55  
56

1  
2  
3 M.G., 2017. Cortical and Subcortical Coordination of Visual Spatial Attention Revealed  
4 by Simultaneous EEG–fMRI Recording. *J. Neurosci.* 37, 7803–7810.

5  
6 doi:10.1523/JNEUROSCI.0326-17.2017  
7

8  
9  
10 Hall, S.D., Holliday, I.E., Hillebrand, A., Singh, K.D., Furlong, P.L., Hadjipapas, A., Barnes,  
11 G.R., 2005. The missing link: Analogous human and primate cortical gamma  
12 oscillations. *Neuroimage* 26, 13–17. doi:10.1016/j.neuroimage.2005.01.009  
13  
14

15  
16  
17 Heidemann, R.M., Ivanov, D., Trampel, R., Fasano, F., Meyer, H., Pfeuffer, J., Turner, R.,  
18  
19 2012. Isotropic submillimeter fMRI in the human brain at 7 T: combining reduced field-  
20 of-view imaging and partially parallel acquisitions. *Magn Reson Med* 68, 1506–1516.  
21  
22 doi:10.1002/mrm.24156  
23  
24

25  
26 Hermes, D., Miller, K.J., Wandell, B. a, Winawer, J., 2014. Stimulus Dependence of Gamma  
27 Oscillations in Human Visual Cortex. *Cereb. Cortex* 1–9. doi:10.1093/cercor/bhu091  
28  
29

30  
31 Hillebrand, A., Barnes, G.R., 2005. Beamformer Analysis of MEG Data. *Int. Rev. Neurobiol.*  
32  
33 doi:10.1016/S0074-7742(05)68006-3  
34  
35

36 Hoogenboom, N., Schoffelen, J.M., Oostenveld, R., Fries, P., 2010. Visually induced  
37 gamma-band activity predicts speed of change detection in humans. *Neuroimage* 51,  
38  
39 1162–1167. doi:10.1016/j.neuroimage.2010.03.041  
40  
41

42  
43 Hoogenboom, N., Schoffelen, J.M., Oostenveld, R., Parkes, L.M., Fries, P., 2006. Localizing  
44 human visual gamma-band activity in frequency, time and space. *Neuroimage* 29, 764–  
45  
46 773. doi:10.1016/j.neuroimage.2005.08.043  
47  
48

49  
50 Horovitz, S.G., Fukunaga, M., De Zwart, J.A., Van Gelderen, P., Fulton, S.C., Balkin, T.J.,  
51  
52 Duyn, J.H., 2008. Low frequency BOLD fluctuations during resting wakefulness and  
53  
54 light sleep: A simultaneous EEG–fMRI study. *Hum. Brain Mapp.* 29, 671–682.  
55  
56

1  
2  
3 doi:10.1002/hbm.20428  
4

5 Howard, M.W., Rizzuto, D.S., Caplan, J.B., Madsen, J.R., Lisman, J., Aschenbrenner-  
6 Scheibe, R., Schulze-Bonhage, A., Kahana, M.J., 2003. Gamma Oscillations Correlate  
7 with Working Memory Load in Humans. *Cereb. Cortex* 13, 1369–1374.  
8  
9

10  
11  
12 doi:10.1093/cercor/bhg084  
13

14 Huster, R.J., Debener, S., Eichele, T., Herrmann, C.S., 2012. Methods for simultaneous EEG-  
15 fMRI: an introductory review. *J Neurosci* 32, 6053–6060.  
16  
17

18  
19 doi:10.1523/JNEUROSCI.0447-12.2012  
20

21 Jung, T.P., Makeig, S., Westerfield, M., Townsend, J., Courchesne, E., Sejnowski, T.J., 2000.  
22 Removal of eye activity artifacts from visual event-related potentials in normal and  
23 clinical subjects. *Clin Neurophysiol* 111, 1745–1758. doi:S1388-2457(00)00386-2 [pii]  
24  
25  
26  
27

28 Jurkiewicz, M.T., Gaetz, W., Bostan, A.C., Cheyne, D., 2006. Post-movement beta rebound  
29 is generated in motor cortex: Evidence from neuromagnetic recordings. *Neuroimage* 32,  
30 1281–1289.  
31  
32  
33  
34

35 Kilavik, B.E., Zaepffel, M., Brovelli, A., MacKay, W.A., Riehle, A., 2013. The ups and  
36 downs of beta oscillations in sensorimotor cortex. *Exp. Neurol.*  
37  
38  
39

40 doi:10.1016/j.expneurol.2012.09.014  
41

42 Laufs, H., Kleinschmidt, A., Beyerle, A., Eger, E., Salek-Haddadi, A., Preibisch, C., Krakow,  
43 K., 2003. EEG-correlated fMRI of human alpha activity. *Neuroimage* 19, 1463–1476.  
44  
45  
46  
47

48 Leicht, G., Vauth, S., Polomac, N., Andreou, C., Rauh, J., Mu??mann, M., Karow, A.,  
49 Mulert, C., 2016. EEG-Informed fMRI Reveals a Disturbed Gamma-Band-Specific  
50 Network in Subjects at High Risk for Psychosis. *Schizophr. Bull.* 42, 239–249.  
51  
52  
53

54 doi:10.1093/schbul/sbv092  
55  
56  
57  
58  
59  
60

- 1  
2  
3 Logothetis, N.K., 2008. What we can do and what we cannot do with fMRI. *Nature* 453,  
4 869–878. doi:10.1038/nature06976  
5  
6  
7  
8 Logothetis, N.K., 2003. The underpinnings of the BOLD functional magnetic resonance  
9 imaging signal. *J Neurosci* 23, 3963–3971.  
10  
11  
12  
13 Logothetis, N.K., Pauls, J., Augath, M., Trinath, T., Oeltermann, A., 2001.  
14 Neurophysiological investigation of the basis of the fMRI signal. *Nature* 412, 150–157.  
15 doi:10.1038/35084005  
16  
17  
18  
19  
20 Magri, C., Schridde, U., Murayama, Y., Panzeri, S., Logothetis, N.K., 2012. The amplitude  
21 and timing of the BOLD signal reflects the relationship between local field potential  
22 power at different frequencies. *J Neurosci* 32, 1395–1407. doi:32/4/1395 [pii]  
23 10.1523/JNEUROSCI.3985-11.2012  
24  
25  
26  
27  
28  
29 Mandelkow, H., Halder, P., Boesiger, P., Brandeis, D., 2006. Synchronization facilitates  
30 removal of MRI artefacts from concurrent EEG recordings and increases usable  
31 bandwidth. *Neuroimage* 32, 1120–1126. doi:10.1016/j.neuroimage.2006.04.231  
32  
33  
34  
35  
36  
37  
38  
39  
40  
41  
42  
43  
44  
45  
46  
47  
48  
49  
50  
51  
52  
53  
54  
55  
56  
57  
58  
59  
60
- Mantini, D., Perrucci, M.G., Del Gratta, C., Romani, G.L., Corbetta, M., 2007.  
Electrophysiological signatures of resting state networks in the human brain. *Proc Natl  
Acad Sci U S A* 104, 13170–13175. doi:10.1073/pnas.0700668104
- Mayhew, S.D., Dirckx, S.G., Niazy, R.K., Iannetti, G.D., Wise, R.G., 2010. EEG signatures  
of auditory activity correlate with simultaneously recorded fMRI responses in humans.  
*Neuroimage* 49, 849–864. doi:10.1016/j.neuroimage.2009.06.080
- Mayhew, S.D., Li, S., Kourtzi, Z., 2012. Learning acts on distinct processes for visual form  
perception in the human brain. *J. Neurosci.* 32, 775–86. doi:10.1523/JNEUROSCI.2033-  
11.2012

- 1  
2  
3 Mayhew, S.D., Ostwald, D., Porcaro, C., Bagshaw, A.P., 2013. Spontaneous EEG alpha  
4  
5 oscillation interacts with positive and negative BOLD responses in the visual-auditory  
6  
7 cortices and default-mode network. *Neuroimage* 76, 362–372.  
8  
9 doi:10.1016/j.neuroimage.2013.02.070  
10  
11  
12 Maziero, D., Velasco, T.R., Hunt, N., Payne, E., Lemieux, L., Salmon, C.E.G., Carmichael,  
13  
14 D.W., 2016. Towards motion insensitive EEG-fMRI: Correcting motion-induced  
15  
16 voltages and gradient artefact instability in EEG using an fMRI prospective motion  
17  
18 correction (PMC) system. *Neuroimage* 138, 13–27.  
19  
20 doi:10.1016/j.neuroimage.2016.05.003  
21  
22  
23 Medicines and Healthcare Products Regulatory Agency, 2015. Safety Guidelines for  
24  
25 Magnetic Resonance Imaging Equipment in Clinical Use.  
26  
27  
28 Michels, L., Bucher, K., Lüchinger, R., Klaver, P., Martin, E., Jeanmonod, D., Brandeis, D.,  
29  
30 2010. Simultaneous EEG-fMRI during a working memory task: Modulations in low and  
31  
32 high frequency bands. *PLoS One* 5, 1–15. doi:10.1371/journal.pone.0010298  
33  
34  
35 Miller, K.J., Leuthardt, E.C., Schalk, G., Rao, R.P.N., Anderson, N.R., Moran, D.W., Miller,  
36  
37 J.W., Ojemann, J.G., 2007. Spectral Changes in Cortical Surface Potentials during  
38  
39 Motor Movement. *J. Neurosci.* 27, 2424–2432. doi:10.1523/JNEUROSCI.3886-06.2007  
40  
41  
42 Mobascher, A., Brinkmeyer, J., Warbrick, T., Musso, F., Wittsack, H.J., Saleh, A., Schnitzler,  
43  
44 A., Winterer, G., 2009. Laser-evoked potential P2 single-trial amplitudes covary with  
45  
46 the fMRI BOLD response in the medial pain system and interconnected subcortical  
47  
48 structures. *Neuroimage* 45, 917–926. doi:10.1016/j.neuroimage.2008.12.051  
49  
50  
51  
52 Moeller, S., Yacoub, E., Olfman, C.A., Auerbach, E., Strupp, J., Harel, N., Ugurbil, K., 2010.  
53  
54 Multiband multislice GE-EPI at 7 tesla, with 16-fold acceleration using partial parallel  
55  
56 imaging with application to high spatial and temporal whole-brain fMRI. *Magn Reson*  
57  
58  
59  
60

1  
2  
3 Med 63, 1144–1153. doi:10.1002/mrm.22361  
4

5 Moosmann, M., Schönfelder, V.H., Specht, K., Scheeringa, R., Nordby, H., Hugdahl, K.,  
6  
7 2009. Realignment parameter-informed artefact correction for simultaneous EEG-fMRI  
8  
9 recordings. *Neuroimage* 45, 1144–1150. doi:10.1016/j.neuroimage.2009.01.024  
10  
11

12 Mukamel, R., Gelbard, H., Arieli, A., Hasson, U., Fried, I., Malach, R., 2005. Coupling  
13  
14 between neuronal firing, field potentials, and FMRI in human auditory cortex. *Science*  
15  
16 309, 951–954. doi:10.1126/science.1110913  
17  
18

19 Mulert, C., Leicht, G., Hepp, P., Kirsch, V., Karch, S., Pogarell, O., Reiser, M., Hegerl, U.,  
20  
21 Jäger, L., Moller, H.J., McCarley, R.W., 2010. Single-trial coupling of the gamma-band  
22  
23 response and the corresponding BOLD signal. *Neuroimage* 49, 2238–2247.  
24  
25 doi:10.1016/j.neuroimage.2009.10.058  
26  
27

28 Mullinger, K.J., Bowtell, R., 2011. Combining EEG and FMRI. *Methods Mol. Biol.* 711,  
29  
30 303–326.  
31  
32

33 Mullinger, K.J., Debener, S., Coxon, R., Bowtell, R., 2008a. Effects of simultaneous EEG  
34  
35 recording on MRI data quality at 1.5, 3 and 7 tesla. *Int. J. Psychophysiol.* 67, 178–188.  
36  
37 doi:10.1016/j.ijpsycho.2007.06.008  
38  
39

40 Mullinger, K.J., Mayhew, S.D., Bagshaw, A.P., Bowtell, R., Francis, S.T., 2014. Evidence  
41  
42 that the negative BOLD response is neuronal in origin: a simultaneous EEG-BOLD-  
43  
44 CBF study in humans. *Neuroimage* 94, 263–274.  
45  
46  
47

48 Mullinger, K.J., Mayhew, S.D., Bagshaw, A.P., Bowtell, R., Francis, S.T., 2013.  
49  
50 Poststimulus undershoots in cerebral blood flow and BOLD fMRI responses are  
51  
52 modulated by poststimulus neuronal activity. *Proc Natl Acad Sci U S A* 110, 13636–  
53  
54 13641. doi:10.1073/pnas.1221287110  
55  
56  
57



- 1  
2  
3 Mullinger, K.J., Morgan, P.S., Bowtell, R.W., 2008b. Improved artifact correction for  
4  
5 combined electroencephalography/functional MRI by means of synchronization and use  
6  
7 of vectorcardiogram recordings. *J Magn Reson Imaging* 27, 607–616.  
8  
9 doi:10.1002/jmri.21277  
10  
11  
12 Mullinger, K.J., Yan, W.X., Bowtell, R., 2011. Reducing the gradient artefact in  
13  
14 simultaneous EEG-fMRI by adjusting the subject's axial position. *Neuroimage* 54,  
15  
16 1942–1950. doi:S1053-8119(10)01281-4 [pii] 10.1016/j.neuroimage.2010.09.079  
17  
18  
19 Murta, T., Hu, L., Tierney, T.M., Chaudhary, U.J., Walker, M.C., Carmichael, D.W.,  
20  
21 Figueiredo, P., Lemieux, L., 2016. A study of the electro-haemodynamic coupling using  
22  
23 simultaneously acquired intracranial EEG and fMRI data in humans. *Neuroimage* 142,  
24  
25 371–380. doi:10.1016/j.neuroimage.2016.08.001  
26  
27  
28 Muthukumaraswamy, S.D., 2013. High-frequency brain activity and muscle artifacts in  
29  
30 MEG/EEG: a review and recommendations. *Front. Hum. Neurosci.* 7, 1–11.  
31  
32 doi:10.3389/fnhum.2013.00138  
33  
34  
35 Muthukumaraswamy, S.D., 2010. Functional Properties of Human Primary Motor Cortex  
36  
37 Gamma Oscillations. *J. Neurophysiol.* 104, 2873–2885. doi:10.1152/jn.00607.2010  
38  
39  
40 Muthukumaraswamy, S.D., Edden, R.A.E., Jones, D.K., Swettenham, J.B., Singh, K.D.,  
41  
42 2009. Resting GABA concentration predicts peak gamma frequency and fMRI  
43  
44 amplitude in response to visual stimulation in humans. *Proc Natl Acad Sci U S A* 106,  
45  
46 8356–8361. doi:10.1073/pnas.0900728106  
47  
48  
49 Muthukumaraswamy, S.D., Singh, K.D., 2013. Visual gamma oscillations: The effects of  
50  
51 stimulus type, visual field coverage and stimulus motion on MEG and EEG recordings.  
52  
53 *Neuroimage* 69, 223–230. doi:10.1016/j.neuroimage.2012.12.038  
54  
55  
56  
57  
58  
59  
60

- 1  
2  
3 Muthukumaraswamy, S.D., Singh, K.D., Swettenham, J.B., Jones, D.K., 2010. Visual gamma  
4 oscillations and evoked responses: variability, repeatability and structural MRI  
5 correlates. *Neuroimage* 49, 3349–3357. doi:10.1016/j.neuroimage.2009.11.045  
6  
7  
8  
9  
10 Niessing J, Ebisch B, Schmidt K, Niessing M, Singer W, Galuske R, 2005. Hemodynamic  
11 Signals Correlate Tightly with Synchronized Gamma Oscillations. *Science* (80-. ). 309,  
12 948–951. doi:10.1126/science.1110948  
13  
14  
15  
16  
17 Nir, Y., Fisch, L., Mukamel, R., Gelbard-Sagiv, H., Arieli, A., Fried, I., Malach, R., 2007.  
18 Coupling between Neuronal Firing Rate, Gamma LFP, and BOLD fMRI Is Related to  
19 Interneuronal Correlations. *Curr. Biol.* 17, 1275–1285. doi:10.1016/j.cub.2007.06.066  
20  
21  
22  
23  
24 Norris, D.G., Koopmans, P.J., Boyaciu??lu, R., Barth, M., 2011. Power independent of  
25 number of slices (PINS) radiofrequency pulses for low-power simultaneous multislice  
26 excitation. *Magn. Reson. Med.* 66, 1234–1240. doi:10.1002/mrm.23152  
27  
28  
29  
30  
31 Novitskiy, N., Ramautar, J.R., Vanderperren, K., De Vos, M., Mennes, M., Mijovic, B.,  
32 Vanrumste, B., Stiers, P., Van den Bergh, B., Lagae, L., Sunaert, S., Van Huffel, S.,  
33 Wagemans, J., 2011. The BOLD correlates of the visual P1 and N1 in single-trial  
34 analysis of simultaneous EEG-fMRI recordings during a spatial detection task.  
35 *Neuroimage* 54, 824–835. doi:10.1016/j.neuroimage.2010.09.041  
36  
37  
38  
39  
40  
41  
42  
43 Olafsson, V., Kundu, P., Wong, E.C., Bandettini, P.A., Liu, T.T., 2015. Enhanced  
44 identification of BOLD-like components with multi-echo simultaneous multi-slice  
45 (MESMS) fMRI and multi-echo ICA. *Neuroimage*.  
46  
47  
48  
49  
50  
51  
52 Olbrich, S., Mulert, C., Karch, S., Trenner, M., Leicht, G., Pogarell, O., Hegerl, U., 2009.  
53 EEG-vigilance and BOLD effect during simultaneous EEG/fMRI measurement.  
54 *Neuroimage* 45, 319–332. doi:10.1016/j.neuroimage.2008.11.014  
55  
56  
57  
58  
59  
60

- 1  
2  
3 Oostenveld, R., Fries, P., Maris, E., Schoffelen, J.M., 2011. FieldTrip: Open source software  
4 for advanced analysis of MEG, EEG, and invasive electrophysiological data. *Comput*  
5  
6  
7 *Intell Neurosci* 2011, 156869. doi:10.1155/2011/156869  
8  
9
- 10 Pantev, C., Makeig, S., Hoke, M., Galambos, R., Hampson, S., Gallen, C., 1991. Human  
11  
12 auditory evoked gamma-band magnetic fields. *Proc. Natl. Acad. Sci. U. S. A.* 88, 8996–  
13  
14 9000. doi:10.1073/pnas.88.20.8996  
15  
16
- 17 Pogosyan, A., Gaynor, L.D., Eusebio, A., Brown, P., 2009. Boosting Cortical Activity at  
18  
19 Beta-Band Frequencies Slows Movement in Humans. *Curr. Biol.* 19, 1637–1641.  
20  
21 doi:10.1016/j.cub.2009.07.074  
22  
23
- 24 Ritter, P., Becker, R., Graefe, C., Villringer, A., 2007. Evaluating gradient artifact correction  
25  
26 of EEG data acquired simultaneously with fMRI. *Magn. Reson. Imaging* 25, 923–932.  
27  
28 doi:10.1016/j.mri.2007.03.005  
29  
30
- 31 Ritter, P., Moosmann, M., Villringer, A., 2009. Rolandic alpha and beta EEG rhythms'  
32  
33 strengths are inversely related to fMRI-BOLD signal in primary somatosensory and  
34  
35 motor cortex. *Hum Brain Mapp* 30, 1168–1187. doi:10.1002/hbm.20585  
36  
37
- 38 Robinson, S.E., Vrba, J., 1999. Functional neuroimaging by synthetic aperture magnetometry  
39  
40 (SAM). *Recent Adv. Biomagn. Tohoku Uni*, 302–305.  
41  
42
- 43 Rosa, M.J., Kilner, J., Blankenburg, F., Josephs, O., Penny, W., 2010. Estimating the transfer  
44  
45 function from neuronal activity to BOLD using simultaneous EEG-fMRI. *Neuroimage*  
46  
47 49, 1496–1509. doi:10.1016/j.neuroimage.2009.09.011  
48  
49
- 50 Schadow, J., Lenz, D., Dettler, N., Fründ, I., Herrmann, C.S., 2009. *NeuroImage Early*  
51  
52 gamma-band responses reflect anticipatory top-down modulation in the auditory  
53  
54 cortex. *Neuroimage* 47, 651–658. doi:10.1016/j.neuroimage.2009.04.074  
55  
56  
57  
58  
59  
60

- 1  
2  
3 Scheeringa, R., Fries, P., Petersson, K.-M., Oostenveld, R., Grothe, I., Norris, D.G., Hagoort,  
4  
5 P., Bastiaansen, M.C.M., 2011. Neuronal Dynamics Underlying High- and Low-  
6  
7 Frequency EEG Oscillations Contribute Independently to the Human BOLD Signal.  
8  
9 Neuron 69, 572–583. doi:10.1016/j.neuron.2010.11.044  
10  
11  
12 Scheibe, C., Ullsperger, M., Sommer, W., Heekeren, H.R., 2010. Effects of parametrical and  
13  
14 trial-to-trial variation in prior probability processing revealed by simultaneous  
15  
16 electroencephalogram/functional magnetic resonance imaging. J Neurosci 30, 16709–  
17  
18 16717. doi:30/49/16709 [pii] 10.1523/JNEUROSCI.3949-09.2010  
19  
20  
21 Schoffelen, J., Oostenveld, R., Fries, P., 2005. Neuronal coherence as a mechanism of  
22  
23 effective corticospinal interaction. Science 308, 111–113. doi:10.1126/science.1107027  
24  
25  
26 Scholvinck, M.L., Maier, A., Ye, F.Q., Duyn, J.H., Leopold, D.A., 2010. Neural basis of  
27  
28 global resting-state fMRI activity. Proc Natl Acad Sci U S A 107, 10238–10243.  
29  
30 doi:0913110107 [pii] 10.1073/pnas.0913110107  
31  
32  
33 Singer, W., Gray, C.M., 1995. Visual Feature Integration and the Temporal Correlation  
34  
35 Hypothesis. Annu. Rev. Neurosci. 18, 555–586. doi:10.1146/annurev.neuro.18.1.555  
36  
37  
38 Stevenson, C.M., Brookes, M.J., Morris, P.G., 2011.  $\beta$ -Band correlates of the fMRI BOLD  
39  
40 response. Hum. Brain Mapp. 32, 182–197. doi:10.1002/hbm.21016  
41  
42  
43 Sumiyoshi, A., Suzuki, H., Ogawa, T., Riera, J.J., Shimokawa, H., Kawashima, R., 2012.  
44  
45 Coupling between gamma oscillation and fMRI signal in the rat somatosensory cortex:  
46  
47 Its dependence on systemic physiological parameters. Neuroimage 60, 738–746.  
48  
49 doi:10.1016/j.neuroimage.2011.12.082  
50  
51  
52 Todd, N., Moeller, S., Auerbach, E.J., Yacoub, E., Flandin, G., Weiskopf, N., 2016.  
53  
54 Evaluation of 2D multiband EPI imaging for high-resolution, whole-brain, task-based  
55  
56  
57  
58  
59  
60

- 1  
2  
3 fMRI studies at 3T: Sensitivity and slice leakage artifacts. *Neuroimage* 124, 32–42.  
4  
5 doi:10.1016/j.neuroimage.2015.08.056  
6  
7  
8 van Drongelen, W., Yuchtman, M., Van Veen, B., van Huffelen, A., 1996. A spatial filtering  
9  
10 technique to detect and localize multiple sources in the brain. *Brain Topogr.* 9, 39–49.  
11  
12  
13 van Veen, B.D., van Drongelen, W., Yuchtman, M., Suzuki, A., 1997. Localization of brain  
14  
15 electrical activity via linearly constrained minimum variance spatial filtering.  
16  
17 *Biomedical* 44, 867–880. doi:10.1109/10.623056  
18  
19  
20 Viswanathan, A., Freeman, R.D., 2007. Neurometabolic coupling in cerebral cortex reflects  
21  
22 synaptic more than spiking activity. *Nat Neurosci* 10, 1308–1312. doi:10.1038/nn1977  
23  
24  
25 Winawer, J., Kay, K.N., Foster, B.L., Rauschecker, A.M., Parvizi, J., Wandell, B.A., 2013.  
26  
27 Asynchronous Broadband Signals Are the Principal Source of the BOLD Response in  
28  
29 Human Visual Cortex. *Curr. Biol.* 23, 1145–1153. doi:10.1016/j.cub.2013.05.001  
30  
31  
32 Womelsdorf, T., Fries, P., Mitra, P.P., Desimone, R., 2006. Gamma-band synchronization in  
33  
34 visual cortex predicts speed of change detection. *Nature* 439, 733–736.  
35  
36 doi:10.1038/nature04258  
37  
38  
39 Wong, E., 2012. Optimized phase schedules for minimizing peak RF power in simultaneous  
40  
41 multi-slice RF excitation pulses, in: *Proceedings of the 20th Annual Meeting of*  
42  
43 *ISMRM*. Melbourne, Australia, p. 2209.  
44  
45  
46 Woolrich, M.W., Behrens, T.E., Beckmann, C.F., Jenkinson, M., Smith, S.M., 2004.  
47  
48 Multilevel linear modelling for fMRI group analysis using Bayesian inference.  
49  
50 *Neuroimage* 21, 1732–1747. doi:10.1016/j.neuroimage.2003.12.023  
51  
52 S1053811903007894 [pii]  
53  
54  
55 Yan, W.X., Mullinger, K.J., Brookes, M.J., Bowtell, R., 2009. Understanding gradient  
56  
57  
58  
59  
60

1  
2  
3 artefacts in simultaneous EEG/fMRI. *Neuroimage* 46, 459–471.  
4

5 Yan, W.X., Mullinger, K.J., Geirsdottir, G.B., Bowtell, R., 2010. Physical modeling of pulse  
6 artefact sources in simultaneous EEG/fMRI. *Hum Brain Mapp* 31, 604–620.  
7  
8  
9  
10 doi:10.1002/hbm.20891  
11

12 Zaepffel, M., Trachel, R., Kilavik, B.E., Brochier, T., 2013. Modulations of EEG Beta Power  
13 during Planning and Execution of Grasping Movements. *PLoS One* 8, 1–10.  
14  
15  
16  
17 doi:10.1371/journal.pone.0060060  
18

19 Zhang, Y., Brady, M., Smith, S., 2001. Segmentation of brain MR images through a hidden  
20 Markov random field model and the expectation-maximization algorithm. *IEEE Trans*  
21  
22  
23  
24  
25  
26  
27  
28  
29  
30  
31  
32  
33  
34  
35  
36  
37  
38  
39  
40  
41  
42  
43  
44  
45  
46  
47  
48  
49  
50  
51  
52  
53  
54  
55  
56  
57  
58  
59  
60  
Med Imaging 20, 45–57. doi:10.1109/42.906424

## Figure Captions

**Figure 1.** Schematic of the sparse MB=3 fMRI scanning scheme and the motor task paradigm showing when four abduction movements were performed within the MR gradient quiet period of a single volume, and were followed by a 16s resting baseline interval for each trial. This results in the movements being performed every 18s.

**Figure 2.** Temperature changes at EEG electrodes, cable bundle and a control location on the scanner bore during a 20-minute GE-EPI sequence scan (MB factor = 4, TR/TE=1000/40ms, SENSE=2, slices=48, B1 RMS=1.09 $\mu$ T, SAR/head=22%) using a Philips Achieva 3T MRI scanner. Temperature was calculated relative to an initial 5-minute baseline recording made before the scan started.

**Figure 3.** Spatial maps of tSNR of middle slice of the stack for each subject for sparse image acquisition sequences with MB factor 2 (top row) and 3 (bottom row). The values below the each map show the mean tSNR  $\pm$  SD over all grey matter voxels for a given subject and scan.

**Figure 4.** EMG activity recorded from the right FDI during the passive (-9 to -7.5s) and active (0-1.5s) time windows (here the time windows are concatenated together for visualisation purposes) from three representative subjects. The average timecourse across all trials and runs from a representative subject is shown. Onset of the first auditory cue occurred at 0s relative to index finger abduction movements. Error bars denote standard deviation across runs.

**Figure 5.** Group average (N=10)  $F$ -statistic beamformer maps showing regions exhibiting power increases and decreases in **a)** gamma- and **b)** beta-power, respectively, during the active window (0-1.5s) as compared with the passive window (-9.5-7s). The crosshairs represent the group average of the individual VE locations found in cM1 for the gamma (**a**) and beta (**b**) frequency activity.

1  
2  
3 **Figure 6.** Group mean (N=10) time-frequency spectrograms demonstrating changes in the  
4 EEG signal power in cM1 relative to the passive window (-9 to -7.5s) for **a&b)** gamma ERS  
5 and **c&d)** beta ERD VE location. The passive window was located in an MR quiet period and  
6 before any anticipation of the stimulus. Time is displayed relative to the auditory cue onset.  
7 Spectrograms were calculated with frequency resolution of 2.5Hz with spectral smoothing of  
8  $\pm 10$ Hz. **a&c)** show 18s whole-trial duration, note the residual GAs during fMRI acquisition  
9 periods. **b&d)** show the gamma and beta power responses during the active window (0 to  
10 1.5s) where movement occurred, with the passive window data appended pre-stimulus for  
11 comparison. Colour bars denote the relative change in power from the average power during  
12 the passive window period (baseline measure) of the passive window for each frequency. See  
13 Figure S4 for absolute power changes of same time-frequency spectrograms.  
14  
15  
16  
17  
18  
19  
20  
21  
22  
23  
24  
25

26  
27 **Figure 7.** Group average (N=10) fMRI mixed effects results. Positive correlation of BOLD  
28 signal to the boxcar model of right index finger abduction movements (red-yellow) and areas  
29 of positive gamma-BOLD correlation (green). All correlations are cluster corrected with  $p <$   
30 0.05, masked with motor cortex. The crosshairs represent the peak positive gamma-BOLD  
31 correlation in cM1 (at [-32, -42, 60] mm).  
32  
33  
34  
35  
36  
37  
38  
39  
40  
41  
42  
43  
44  
45  
46  
47  
48  
49  
50  
51  
52  
53  
54  
55  
56  
57  
58  
59  
60



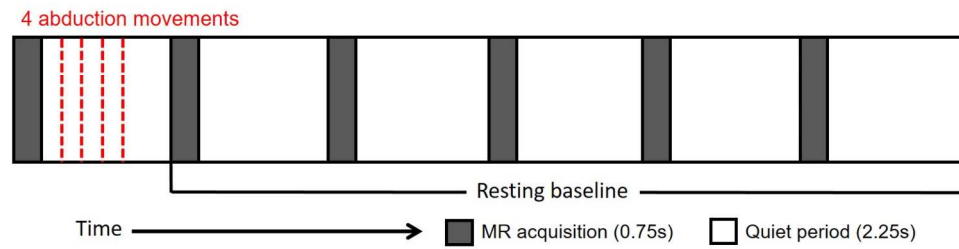


Figure 1: Schematic of the sparse MB=3 fMRI scanning scheme and the motor task paradigm showing when four abduction movements were performed within the MR gradient quiet period of a single volume, and were followed by a 16s resting baseline interval for each trial. This results in the movements being performed every 18s.

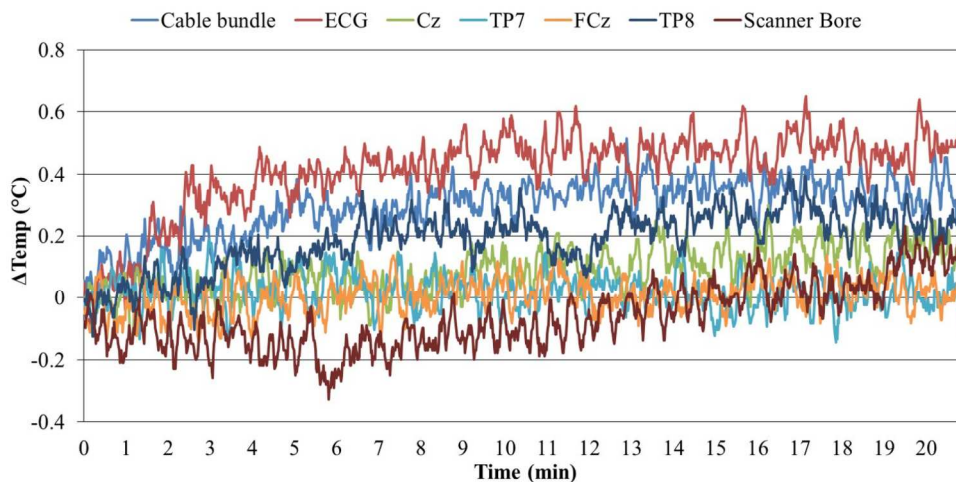


Figure 2: Temperature changes at EEG electrodes, cable bundle and a control location on the scanner bore during a 20-minute GE-EPI sequence scan (MB factor = 4, TR/TE=1000/40ms, SENSE=2, slices=48, B1 RMS=1.09 $\mu$ T, SAR/head=22%) using a Philips Achieva 3T MRI scanner. Temperature was calculated relative to an initial 5-minute baseline recording made before the scan started.

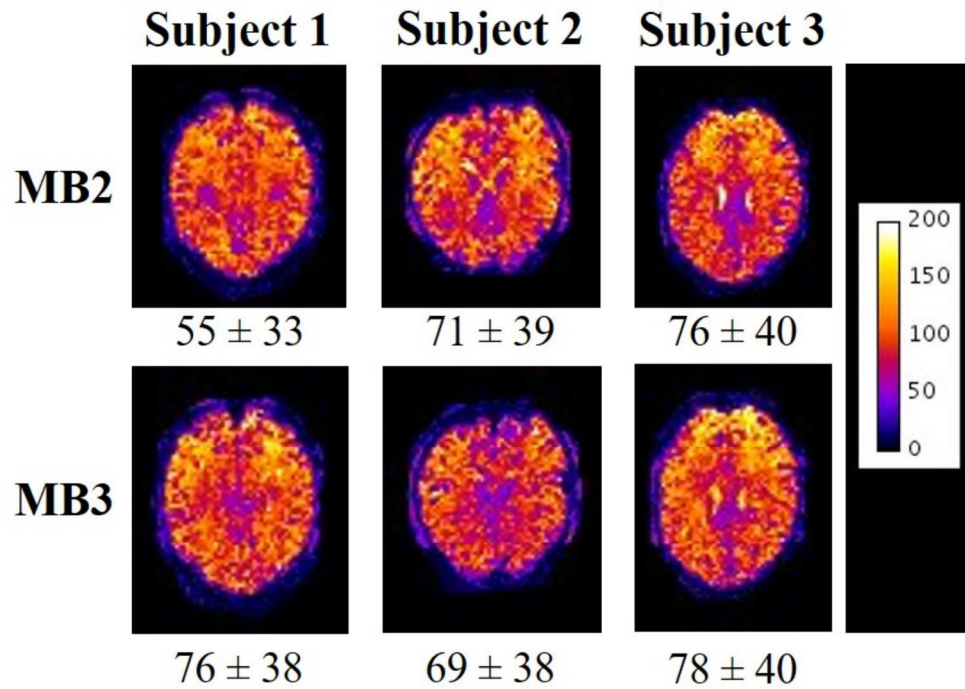


Figure 3: Spatial maps of tSNR of middle slice of the stack for each subject for sparse image acquisition sequences with MB factor 2 (top row) and 3 (bottom row). The values below the each map show the mean tSNR  $\pm$  SD over all grey matter voxels for a given subject and scan.

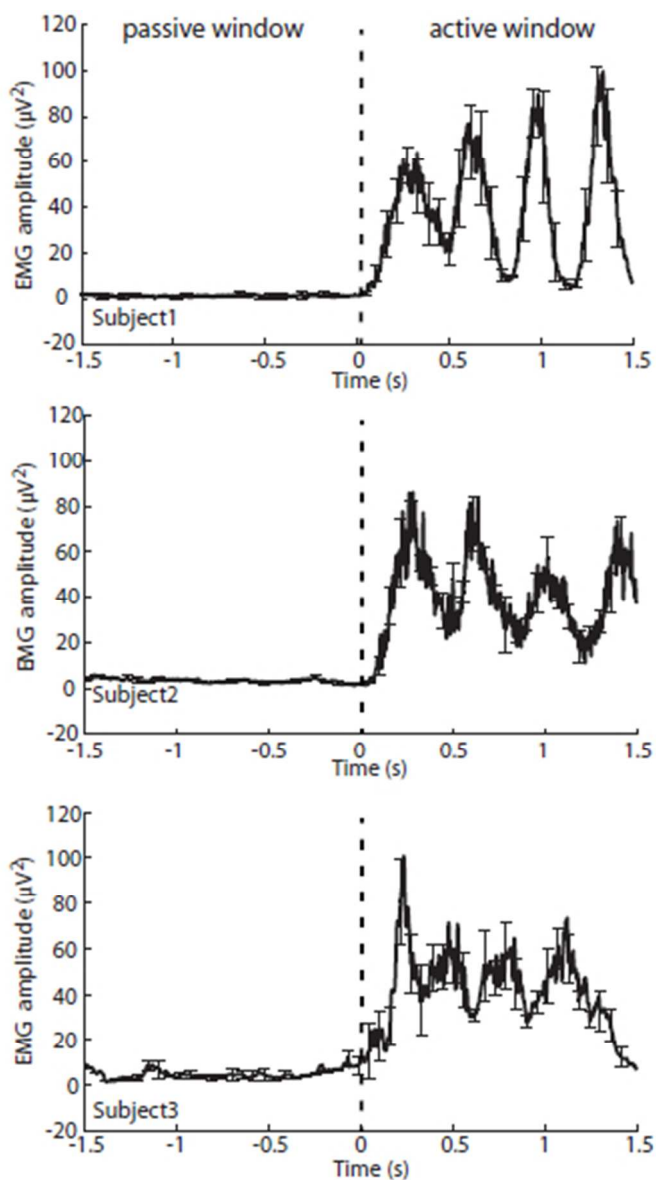
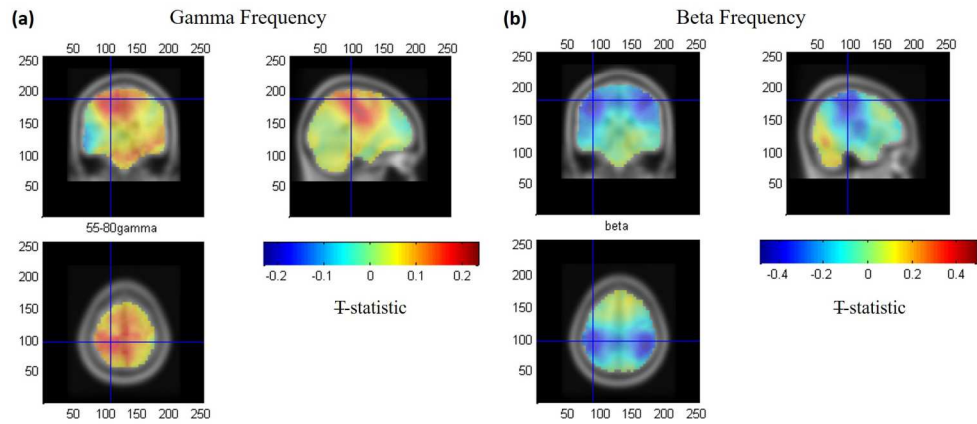


Figure 4. EMG activity recorded from the right FDI during the passive (-9 to -7.5s) and active (0-1.5s) time windows (here the time windows are concatenated together for visualisation purposes) from three representative subjects. The average timecourse across all trials and runs from a representative subject is shown. Onset of the first auditory cue occurred at 0s relative to index finger abduction movements. Error bars denote standard deviation across runs.

90x155mm (96 x 96 DPI)



22 Figure 5: Group average (N=10) T-statistic beamformer maps showing regions exhibiting power increases  
23 and decreases in a) gamma- and b) beta-power, respectively, during the active window (0-1.5s) as  
24 compared with the passive window (-9.5-7s). The crosshairs represent the group average of the individual  
25 VE locations found in cM1 for the gamma (a) and beta (b) frequency activity.

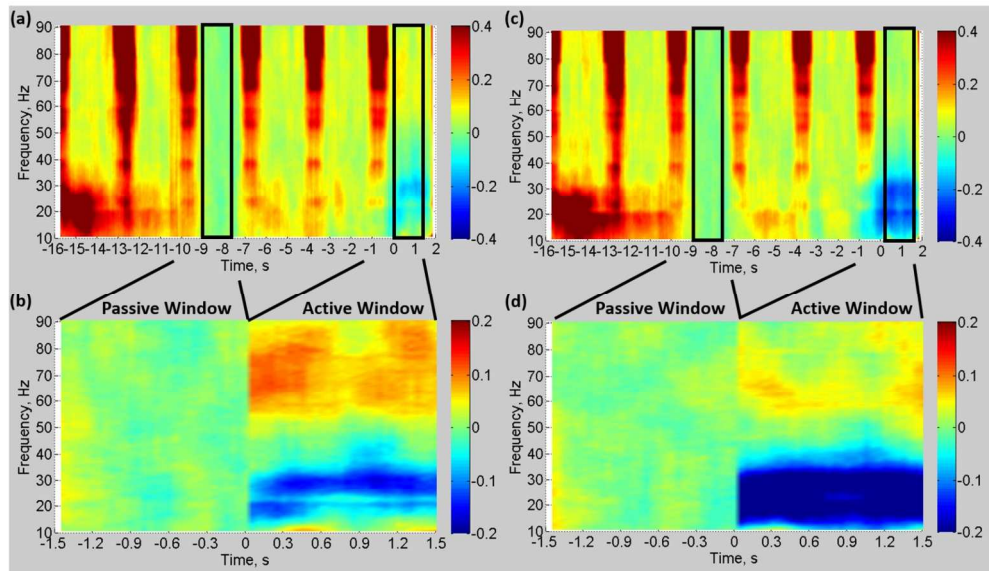
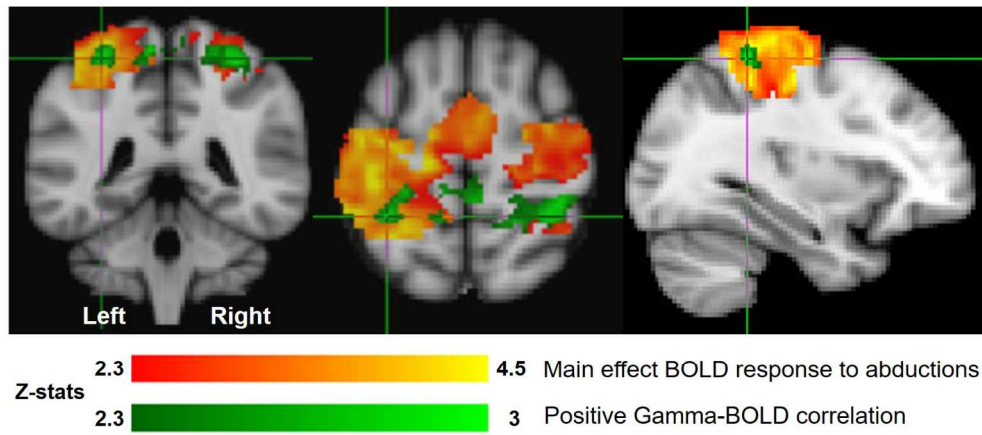


Figure 6: Group mean (N=10) time-frequency spectrograms demonstrating changes in the EEG signal power in cM1 relative to the passive window (-9 to -7.5s) for a&b) gamma ERS and c&d) beta ERD VE location. The passive window was located in an MR quiet period and before any anticipation of the stimulus. Time is displayed relative to the auditory cue onset. Spectrograms were calculated with frequency resolution of 2.5Hz with spectral smoothing of  $\pm 10$ Hz. a&c) show 18s whole-trial duration, note the residual GAs during fMRI acquisition periods. b&d) show the gamma and beta power responses during the active window (0 to 1.5s) where movement occurred, with the passive window data appended pre-stimulus for comparison. Colour bars denote the relative change in power from the average power during the passive window period (baseline measure) of the passive window for each frequency. See Figure S2 for absolute power changes of same time-frequency spectrograms.



22 Figure 7: Group average (N=10) fMRI mixed effects results. Positive correlation of BOLD signal to the boxcar  
23 model of right index finger abduction movements (red-yellow) and areas of positive gamma-BOLD  
24 correlation (green). All correlations are cluster corrected with  $p < 0.05$ , masked with motor cortex. The  
25 crosshairs represent the peak positive gamma-BOLD correlation in cM1 (at [-32, -42, 60] mm).  
26  
27  
28  
29  
30  
31  
32  
33  
34  
35  
36  
37  
38  
39  
40  
41  
42  
43  
44  
45  
46  
47  
48  
49  
50  
51  
52  
53  
54  
55  
56  
57  
58  
59  
60

Multiband Factor	Slice acquisition spacing	tSNR
1	Equidistant	74 ± 40
2	Equidistant	72 ± 39
2	Sparse	67 ± 37
3	Equidistant	68 ± 37
3	Sparse	74 ± 38

**Table 1.** Mean temporal SNR (tSNR) ( $\pm$ standard deviation) calculated over grey matter across 3 participants during five MR sequences: MB: 1-3; acquisition type = equidistant or sparse. All other parameters were constant: TR/TE=3060/40ms, SENSE=2, slices=36, FA=79°, Volumes=41.